

# Kif6 regulates cilia motility and polarity in brain ependymal cells

Maki Takagishi<sup>1</sup>, Yang Yue<sup>2</sup>, Ryan S. Gray<sup>3</sup>, Kristen J. Verhey<sup>2</sup>, and John B. Wallingford<sup>1,\*</sup>

<sup>1</sup>Department of Molecular Biosciences, Patterson Labs, The University of Texas at Austin, Austin, Texas, USA

<sup>2</sup>Department of Cell and Developmental Biology, University of Michigan Medical School, Ann Arbor, MI, 48109, USA

<sup>3</sup>Departments of Nutrition and Pediatrics, Dell Pediatric Research Institute, The University of Texas at Austin, Dell Medical School, Austin, Texas, USA

\*wallingford@austin.utexas.edu (JBW)

**Keywords:** Kinesin, multiple motile cilia, ependymal cell cilia beating, cilia, Kif6

## Summary statement

We found that Kif6 is localized to the axonemes of ependymal cells. In vitro analysis shows that Kif6 moves on microtubules and that its loss in mice decrease cilia motility and cilia-driven flow, resulting in hydrocephalus.

## Abstract

Motile cilia on ependymal cells lining brain ventricular walls beat in concert to generate laminar cerebrospinal fluid (CSF) flow. Dyneins and kinesins are ATPase microtubule motor proteins that promote the rhythmic beating of cilia axonemes. Despite common consensus about the importance of axonemal dynein motor proteins, little is known about how kinesin motors contribute to cilia motility. Here, we show that Kif6 is a slow processive motor ( $12.2 \pm 2.0$  nm/s) on microtubules *in vitro* and localizes to both the apical cytoplasm and the axoneme in ependymal cells, though does not display processive movement *in vivo*. Using a mouse mutant that models a human Kif6 mutation in a proband displaying macrocephaly, hypotonia, and seizures, we find that

loss of Kif6 function caused decreased ependymal cilia motility and subsequently decreased fluid flow on the surface of brain ventricular walls. Disruption of Kif6 also disrupts cilia orientation, the formation of robust apical actin networks, and stabilization of basal bodies at the apical surface. This suggests a novel role for the Kif6 motor in maintenance of ciliary homeostasis in ependymal cells.

## Introduction

Multiciliated cells (MCC) have dozens of motile cilia, which are planar polarized and coordinately beat to generate directional flow across an epithelium (Brooks and Wallingford, 2014). Ciliary-driven directional fluid flow maintains mucus clearance in the respiratory tract, the transport of gametes in the reproductive system, and the cerebrospinal fluid (CSF) circulation in the brain, (Spassky and Meunier, 2017), though recent studies reveal subtle but important differences in these MCC populations (Konjikusic et al., 2018; Roberson et al., 2020)

Dyneins and kinesins are ATPase microtubule motor proteins that drive diverse motion in cilia and flagella (Gennerich and Vale, 2009). For example, axonemal dynein complexes, such as outer and inner dynein arms, are arrayed along microtubule doublets to generate motive force for cilia beating (Ishikawa, 2017). However, while both kinesins and dyneins help facilitate intraflagellar transport of cargoes necessary to build and maintain cilia (Prevo et al., 2017), the function of several ciliary kinesins remains poorly defined (Konjikusic et al., 2021)

For example, the kinesin-9 family contains two subfamilies, kinesin-9A and kinesin-9B (Wickstead et al., 2010), that have been implicated in cilia function but remain only cursorily studied. In *Trypanosoma brucei*, both family members, KIF9A and KIF9B, are localized in the axoneme and their knockdown reduced flagellum motility (Demonchy et al., 2009). The KIF9A homologues *Chlamydomonas reinhardtii* KLP1 and vertebrate Kif9 were recently shown to be active motors that act in the central pair to facilitate ciliary beating (Konjikusic et al., 2023; Han et al., 2022).

Less is known about members of the kinesin-9B subfamily. The vertebrate member Kif6 was implicated in cardiovascular disease in humans (Ruiz-Ramos et al., 2015), though a meta-analysis of multiple case-control studies failed to find evidence of this association (Assimes et al., 2010). Instead, more recent studies in fish, mice, and human suggests a role for Kif6 in cilia in the brain (Gray et al., 2021; Konjikusic et al., 2018). In both zebrafish and mice, loss of Kif6 function is associated with hydrocephalus and decreased cilia numbers in the adult brain ventricles (Gray et al., 2021; Konjikusic et al., 2018), though little else is understood of the cell biology of Kif6 function.

Here, we provide evidence that Kif6 functions as a canonical plus-end directed kinesin motor capable of slow, processive, microtubule-based movement *in vitro*. Loss of Kif6 function in mice elicits a complex array of cilia-related phenotypes in the brain including defects in cilia beating, CSF fluid flow, and planar polarization of basal bodies. Over time, ependymal cilia in Kif6 mutant mice are lost, possibly due to defects in apical actin assembly and subsequent destabilization of basal bodies. Thus, our data suggest that Kif6 plays several roles in ependymal cell cilia homeostasis and neurodevelopment in mammals and may shed light on Kif6-related human pathologies.

## Results

### **Kif6 is an active motor protein that walks towards microtubule plus ends**

We previously reported a macrocephaly patient with a mutation in *KIF6* that lacks part of the coiled-coil stalk region and the C-terminal tail domain (Konjikusic et al., 2018), which is the putative cargo-binding domain (Piddini et al., 2001). We also generated mice with a similar mutation lacking Kif6's C-terminal stalk and tail domains, which displayed variably penetrant hydrocephalus and reduction in ependymal cell cilia (Konjikusic et al., 2018). Since the motor activity of Kif6 has never been determined, these findings led us to perform *in vitro* studies.

The alignment of the protein sequences of human (h), mouse (m), and *Danio rerio* (d) Kif6 proteins showed that the overall domain organization is highly conserved

(Fig. 1A, S1A-B). When overexpressed in COS-7 cells, full-length (FL) mouse Kif6-EGFP did not localize to microtubules but rather showed a diffuse localization within the cytosol (Fig. S1C). In *in vitro* single-molecule motility assays, mKif6 (FL)-EGFP did not bind to taxol stabilized microtubules (Fig. S1D), suggesting that full-length mKif6 is regulated by auto-inhibition, which is common for kinesin proteins (Verhey and Hammond, 2009). To examine the motility properties of mKif6, we generated a truncated version, mKif6 (1-493)-mNeonGreen (mNG), which includes the motor domain and the first two coiled-coil segments for homodimerization (Fig. 1A). When overexpressed in COS-7 cells, mKif6 (1-493)-mNG was found both along microtubules and diffusely in the cytoplasm (Fig. 1B).

To visualize Kif6 movement directly, we carried out *in vitro* single-molecule motility assays and found that mKif6(1-493)-mNG moved processively along microtubules with a speed of  $12.2 \pm 2$  nm/sec (Mean  $\pm$  SD) (Fig. 1C-E, Movie 1). Similar speeds ( $15.5 \pm 4.4$  nm/sec) were obtained with a truncated version of zebrafish Kif6 (not shown). This slow rate of processive movement along microtubule tracks is similar to that reported previously for the related kinesin, Kif9 (Konjikusic et al., 2023).

To test whether the Kif6 proteins move processively towards the plus or the minus ends of microtubules, we repeated the single-molecule motility assays in the presence of the kinesin-3 protein KIF1A as a truncated version of this motor protein, KIF1A(1-393), is known to move with high speed and processivity towards the plus ends of microtubules (Hammond et al., 2009; Soppina et al., 2014). For these experiments, we used KIF1A(1-393) tagged with Halo tag and labeled with the Halo ligand JFX554. Given the differences in speed between the kinesin-3 KIF1A and the kinesin-6 proteins, we first imaged KIF1A motility along microtubules at a rapid frame rate (10 frames per sec) and then the motility of KIF6 proteins along the same microtubule at a slower frame rate (1 frame every 3 sec). Kymographs revealed that both mouse KIF6(1-493)-mNG (Fig. S2) and zebrafish KIF6(1-501)-mNG (not shown) moved in the same direction as KIF1A, demonstrating that they move processively towards the microtubule plus end.

## Kif6 localizes to the cytoplasm and cilia of multiciliated ependymal cells.

We then expressed mKif6 (1-493)-mNG in developing ependymal cells, where it co-localized with  $\beta$ -tubulin not only in cytoplasmic microtubules but also in cilia (Fig. 1F, I). While mKif6 (1-493)-mNG accumulated at the tip of cilia (Fig. 1G, I), we were unable to observe any clear movement of mKif6 (1-493)-mNG within these cilia (Fig. 1H, Movie 2). Together, these data suggest that while the Kif6 motor domain derived from both zebrafish and mice is able to bind to and move processively along microtubules, it may not do so appreciably inside cilia; a similar behavior has been shown for other KIF9 Family kinesins such as *Chlamydomonas* Klp1 and *Xenopus* Kif9 (Konjikusic et al., 2023; Han et al., 2023).

We next set out to define endogenous Kif6 protein localization using immunochemistry. Antibody specificity was confirmed using Western blot analysis of primary ependymal cell lysates derived from WT and *Kif6*<sup>pG555f/pG555f</sup> homozygous mutant mice (hereafter labeled *Kif6*<sup>pG555f</sup>). The *Kif6*<sup>pG555f</sup> mutation is predicted to truncate Kif6 protein thus removing the antigen region of the Kif6 antibody. We confirmed a single band of Kif6 protein expression in testis and in primary cultured ependymal cells by Western blot (Fig 2A). Interestingly, we consistently observed multiple bands using the Kif6 antibody in lysates derived from Lateral Ventricular (LV) wall tissues. Because LV wall tissues contains many cells other than pure populations of primary cultured ependymal cells, robust Kif6 expression may be masked in these lysates. Next, we enriched for ependyma from primary LV tissue and confirmed ependymal cell differentiation at D0, D5, and D14. At D0, the precursor cells had Arl13b-positive a short cilium (primary cilia). At D5, the cultured dish included precursor cells and immature ependymal cells that had short or elongating multiple cilia. At D14, mature ependymal cells had multiple long cilia (Fig. 2B). We first observed Kif6 at D5 of differentiation, which is concomitant with the onset of MCC differentiation in cultured ependymal cells.

We next examined Kif6 localization in ependymal cells by immunostaining *in vivo*. At D5 we observed Kif6 punctum close to primary cilium, with increased accumulation at the base of both short developing and long developed multicilia (Fig. 2C). To resolve these accumulations of Kif6 in multicilia we used super-resolution

imaging in D14 ependymal cell cultures, showing puncta along the length of ciliary axonemes (Fig. 2D). We also observed Kif6 puncta at the apical cell cortex localized with the basal foot marker,  $\gamma$ -tubulin (Fig. 2E), and partially co-localized with microtubules ( $\beta$ -tubulin) at apical cell cortex around the ciliary base (Fig. 2F). The specificity of immunostaining with Kif6 antibody was confirmed by the loss of signal at multicilia in D14 ependymal cells derived from *Kif6*<sup>pG555fs</sup> mutant mice (Fig. 2G). Finally, an exogenously expressed N-terminal fluorescently tagged mCherry-Kif6 protein localized at multicilia and apical cell cortex with  $\beta$ -tubulin (Fig. 2H). These results suggest that endogenous Kif6 localizes at the apical tubulin cortex, at the base of cilia, and within ciliary axonemes.

### **Kif6 regulates cilia motility in ependymal cells**

As noted, *Kif6*<sup>pG555fs</sup> mice display variably penetrant hydrocephalus (Fig. 3A and Konjikusic et al., 2018). We observed moderate hydrocephalus with enlarged LV in 69.2% (9/13 mice) while severe hydrocephalus, often associated with a disrupted LV wall and an absence of ependymal cells, was observed in the remainder (Fig. 3B). Because ependymal cilia were present in the middle part of LV wall in *Kif6*<sup>pG555fs</sup> mice with moderate hydrocephalus (Fig. 3C-D and S3), we chose these for a more detailed analysis of ciliary phenotypes.

As ependymal cilia beating contributes to directional flow and CSF circulation in mouse brain, we first observed the cilia-driven flow on the surface of LV wall (Fig. 3E). Microbeads were placed on the surface of LV wall at the middle part and flowed in a linear path along the anterior-dorsal region in wild-type (WT) LV wall (Fig. 3E, F). On the other hand, bead displacement on *Kif6*<sup>pG555fs</sup> ventricles was significantly slower than WT (Fig. 3G) and more torturous (Fig. 3F, Movie 3-4).

Because knockdown of *Trypanosome* Kif9B (a homolog of Kif6) causes motility defects in the flagellum (Demonchy et al., 2009), we next asked if the *Kif6*<sup>pG555fs</sup> mutation also impairs ependymal cilia beating. To avoid potentially confounding effects of hydrocephalus and other environmental factors within brain ventricles, we evaluated

cilia beating in primary cultured ependymal cells. Live imaging of ependymal cells showed the coordinated cilia beatings in WT and the decreased cilia motility in *Kif6<sup>pG555fs</sup>* (Fig. 3H, Movie 5-7). Consistent with the variable penetrance of hydrocephalus, we found at D14 that *Kif6<sup>pG555fs</sup>* ependymal cells had normal, faint, or no motile cilia (Fig. 3I, Movie 6) and that the beating frequency of ependymal cilia, when present, were significantly decreased in *Kif6<sup>pG555fs</sup>* compared with WT cilia (Fig. 3J). Interestingly, cilia beat frequency in *Kif6<sup>pG555fs</sup>* was not significantly different with D21 WT (Fig. 3J), suggesting that cilia beating in *Kif6<sup>pG555fs</sup>* was restored as ependymal cells mature. Moreover, we found that the percentage of ependymal cells with immotile cilia was decreased in D21 *Kif6* mutant (Fig. S4A). The remaining *Kif6<sup>pG555fs</sup>* ependymal cells at D21 had normal apical actin networks (Fig. S4B-D) and better BB orientation (Fig. S4E-F) than the population of *Kif6* mutant ependymal cells at D14. Thus, *Kif6* appears to play a stage-dependent role in organizing directional ciliary beating.

As kinesins can form homo- and hetero-dimers, kinesins without the motor domain (motor-less) can act as dominant negative proteins (Gelfand et al., 2001). To test this model, we transfected a N-terminal tagged motor-less *Kif6* construct (mCherry-*Kif6* ML) into ependymal cells. We observed that mCherry-*Kif6* ML significantly suppressed cilia beatings in D14 ependymal cells compared with mCherry control (Fig. 3K-L, Movie 8-9). These results suggest that *Kif6* regulates cilia motility in ependymal cells.

### **Ependymal cilia in *Kif6<sup>pG555fs</sup>* display relatively normal axoneme ultrastructure**

Cilia motility requires a radially-arranged nine doublet microtubules and axonemal dyneins in repeating patterns (Ma et al., 2019). To observe if ultrastructural defects may explain the decrease cilia beat frequency, we visualized cilia structure in WT and *Kif6<sup>pG555fs</sup>* mutant mice by Transmission Electron Microscopy (TEM). TEM images showed a typical 9+2 arrangement with outer dynein arms in both WT and *Kif6<sup>pG555fs</sup>* ependymal cilia at P14 (Fig. 4A and S5). Using immunofluorescence we show that the outer dynein arm component *Dna11* was present in *Kif6<sup>pG555fs</sup>* ependymal

cell cilia as in WT (Fig. 4B-C). Decreased cilia length is associated with decreased cilia motility (Bottier et al., 2019), however we found that the length of *Kif6*<sup>pG555fs</sup> ependymal cilia, when present, was not significantly different from control (Fig. 4D-E). Finding no overt structural defects in *Kif6*<sup>pG555fs</sup> ependymal cilia, we turned our attention to the MCC apical cytoplasm.

### ***Kif6* is required for planar polarization of ependymal cells**

Because Kif6 was localized to apical cytoplasmic microtubules, we next analyzed the apical microtubules that in ependymal cells form an organized network and align the basal bodies (BB's) (Werner et al., 2011; Kunitomo et al., 2012). Because Kif19A is known to depolymerize microtubules (Niwa et al., 2012), we first examined general microtubule organization in *Kif6*<sup>pG555fs</sup> ependymal cells, but overexpression of mCherry-Kif6 full length or the dominant negative Kif6 ML had no effect on acetylated-tubulin, which correlates with stable microtubules, in ependymal cell bodies (Fig. S6). Moreover, *Kif6*<sup>pG555fs</sup> did not diminish the intensity of  $\beta$ -tubulin labeled microtubule accumulation around BBs (Fig. 5A, B).

Because the surface flow was disturbed on *Kif6*<sup>pG555fs</sup> LV wall (Fig. 3F), we next analyzed cilia polarity/orientation at the single cell level (rotational polarity) and at the tissue level (translational polarity) (Mirzadeh et al., 2010). Rotational polarity was quantified by the orientation of the basal foot (BF) projection from BB. Using TEM of P14 LV walls, we showed that the orientation of the BF-BB was perturbed *Kif6*<sup>pG555fs</sup> compared to parallel orientation typically observed in WT (Fig.5C). We also observed this rotational polarity defect in cultured ependymal cells derived from *Kif6*<sup>pG555fs</sup> mutants by immunostaining with FGFR1 Oncogene Partner (FOP, a BB marker) and  $\gamma$ -tubulin (a BF marker) (Fig. 5D). The orientation of BB-BF alignments in the plane of D14 cultured ependymal cells, was calculated as mean resultant vector lengths (R bar) and was found to be significantly reduced in *Kif6*<sup>pG555fs</sup> ependymal cells (Fig.5E).

Ependymal cilia also display translational polarity, visible as the clustering of BB on the LV wall along the direction of CSF flow (Ohata and Alvarez-Buylla, 2016).

We observed BB clustering within each ependymal cell at the anterior-dorsal area of LV walls, finding them positioned ventrally (Fig.5F). This translational polarity was disturbed in *Kif6*<sup>pG555fs</sup> (Fig. 5G). BB clustering was quantified as vector angles from the center of the cell to the center of the multicilia bundle base (Fig. 5H), which was more randomly distributed in *Kif6*<sup>pG555fs</sup> LV walls compared with the polarized distribution observed in WT tissues (Fig. 5I). BB clusters in *Kif6*<sup>pG555fs</sup> mutants were close to the center of cell (Fig. 5J) and the directionality was significantly decreased (Fig. 5K).

Finally, tyrosinated-tubulin, which marks newly polymerized microtubule plus ends, is asymmetrically localized to apical junctions in ependymal cells, and this microtubule polarization promotes cilia polarity (Takagishi et al., 2020). However, *Kif6*<sup>pG555fs</sup> LV walls showed the normal asymmetric localization of tyrosinated-tubulin (Fig. 5G). We also observed no difference in the intensity of tyrosinated-tubulin between *Kif6*<sup>pG555fs</sup> and WT (Fig.5L). On the other hand, the directionality of BB clusters toward the polarized tyrosinated-tubulin was significantly decreased in *Kif6*<sup>pG555fs</sup> (Fig.5M-N). These results suggest that Kif6 affect cilia polarity independently of the apical microtubules.

### Loss of Kif6 function affects apical actin assembly and BB stability

Apical actin forms networks in MCC that aid in connecting BBs and contributing to their alignment, orientation, and stabilization in MCC (Werner et al., 2011; Mahuzier et al., 2018). Using fluorescently labelled phalloidin, which labels actin filaments, we observed apical actin accumulation co-localized with BBs in both WT and *Kif6*<sup>pG555fs</sup> LV tissues (Fig. 6A). However, we observed a significant decrease in actin accumulation localized with BB clusters in *Kif6*<sup>pG555fs</sup> mutants (Fig. 6B). Moreover, the area of BB clusters was significantly increased in *Kif6*<sup>pG555fs</sup> ependymal cell (Fig. 6C) and were dispersed across the apical cell cortex with decreased apical actin, compared to the tight accumulation of BBs in WT ependymal cells (Fig.6A). Importantly, the loss of apical actin networks has been shown to induce BB dis-attachment in ependymal cells (Mahuzier et al., 2018). Accordingly, we found that the number of BBs was significantly decreased in *Kif6*<sup>pG555fs</sup> ependymal cells (Fig. 6D). Because the BBs were

not found in deeper cytoplasm (Fig. 6E), these results suggest that the defect of apical actin networks in *Kif6*<sup>pG555fs</sup> may cause the de-stabilization of BBs and shedding of ependymal cilia.

## Discussion

Here, we describe a complex of cilia-related defects in the ependymal cells of *Kif6* mutant mice. We suggest that this complex phenotype emerges from pleiotropic defects in ependymal cells. Because *Kif6* actively moves along microtubules and is present in axonemes (Fig. 1), defects in cilia beating may result from the direct action of *Kif6* in cilia motility. Conversely, because we demonstrate that *Kif6* is required for apical actin assembly, its presence in the apical cytoplasm may explain defects in cilia polarity. Finally, we suggest that the defects in apical actin assembly may also result in the loss of cilia from ependymal cells. Together, this constellation of ciliary defects results in defective CSF flow and moderate hydrocephalus in *Kif6* mutant mice (Fig. 6F).

We have shown here that the kinesin-9B family member *Kif6* is a slow processive motor *in vitro* yet we were unable to observe processive movement of the protein in cilia *in vivo*. In this way, *Kif6* closely resembles the related kinesin-9A protein *Kif9* in undergoing slow, processive motility *in vitro* but not inside cilia (Konjikusic et al., 2023). In addition, processive movement in axonemes of another kinesin-9A family member, *Chlamydomonas* *Klp1*, also could not be observed (Han et al., 2023). One possibility is that the slow motility of kinesin-9 proteins evolved to permit nucleotide-dependent engagement and disengagement with central pair microtubules and thereby contribute to ciliary bending in a manner analogous to how the non-processive axonemal dyneins engage with doublet microtubules (Han et al., 2023). Alternatively, the motility of kinesin-9 motor proteins in axonemes may be hindered given that the central pair microtubules are decorated by a tight array of associated proteins that do not appear to leave any unoccupied surface for processive movement of a kinesin (Yokoyama et al., 2004).

The defects in cilia motility that we report here in Kif6 mutant mice may relate to the cilia motility defects observed after knockdown of *Trypanosome KIF9B*, which disrupts beating and formation of the paraflagellar rod (PFR) within the flagellar membrane (Demonchy et al., 2009). However, since mammalian ependymal cilia don't have an analogous PFR structure, the precise locale of Kif6 action in the vertebrate axoneme remains to be determined. One possibility is that Kif6 acts in the central pair, similar to the kinesin-9As vertebrate Kif9 and *Chlamydomonas* Klp1 (Konjikusic et al., 2023; Han et al., 2022). This possibility is supported by recent protein interactome mapping in *Tetrahymena* using cross-linking mass-spectrometry, which identified links between Kif6 and the central pair protein Spag16 and the nearby radial spoke head protein Rsph4 (McCafferty et al., 2023). In fact, some redundancy between Kif6 and Kif9 might explain the finding that *Kif6<sup>p.G555fs</sup>* ependymal cilia display decreased motility at D14, but recovered by D21 (Fig. 1J).

Kif6 mutation affected not only cilia motility but also cilia polarity (Fig. 5), and these polarity defects likely contribute to the disturbed flow over LV wall (Fig. 3F). Cilia orientation is regulated by apical microtubules (Vladar et al., 2012; Takagishi et al., 2020) and affected by apical actin networks between BBs (Werner et al., 2011), so Kif6 localization to this region is of interest as it marks a clear departure from that observed for Kif9 (Konjikusic et al., 2023). However, Kif6 mutation did not affect the overall appearance of apical microtubules (Fig. 5 and S6), suggesting disturbed cilia polarity might be secondary to the defects in cilia motility.

Indeed, cilia beating motility induces apical actin network organization that is crucial for BB stabilization (Mahuzier et al., 2018). Suppressed cilia motility would be expected to result in decreased apical actin networks around BBs, and de-stabilized BBs could be dis-attached (Mahuzier et al., 2018). Because we observed all of these phenotypes, it is possible that despite the presence of Kif6 in the apical cytoplasm, that Kif6-related actin defects are secondary to cilia beating defects. A final possibility is that Kif6 mutant ependymal cilia with decreased motility are physically removed (by shedding) because of BB de-stabilization, as suggested by Mahuzier et al., 2018 (Fig. 6D-F), and that stable cilia that remain until D21 display normal beating.

## Materials and Methods

### Mouse experiments

*Kif6*<sup>pG555fs</sup> mice were generated using CRISPR-Cas9 system (Konjikusic et al., 2018). *Kif6*<sup>pG555fs</sup> or C57Bl/6J mice were used for whole-mount staining, ependymal cell culture, and LV explants cultures. All mice were maintained with 12/12 h light/dark cycle and no more than 5 mice per cage. Both male and female mice were used for the experiments, and sex differences were not observed. All mouse experiments were approved by the Animal Studies Committee at University of Texas at Austin (AUP-2021-00118).

### Plasmids

Mouse Kif6 cDNA encodes 803 amino acid protein (NP\_796026) was cloned from a mouse brain cDNA library and sequenced. The cDNAs of mKif6 FL (1-803aa) and ML (360-803aa) were subcloned into pEGFP-C1 vector or pmCherry2-C1 vector (a gift from Michael Davidson, Addgene plasmid # 54563). mCherry was removed and mKif6 (1-493aa)-mNeonGreen was added into pmCherry2 vector.

### Cell culture, transfection and lysate preparation

COS-7 (monkey kidney fibroblast) cells obtained from ATCC (RRID: CVCL\_0224) were cultured in DMEM (Gibco) with 10% (vol/vol) Fetal Clone III (HyClone) and 1% GlutaMAX (Gibco) at 37°C with 5% CO<sub>2</sub>. COS-7 cells were transfected with Trans-IT LT1 (Mirus) according to the manufacturer's instructions.

COS-7 cells were collected 48 h post-transfection. The cells were harvested by low-speed centrifugation at 1,500 × g for 5 min at 4°C. The pellet was rinsed once in PBS and resuspended in ice-cold lysis buffer (25 mM HEPES/KOH, 115 mM potassium acetate, 5 mM sodium acetate, 5 mM MgCl<sub>2</sub>, 0.5 mM EGTA, and 1% Triton X-100, pH 7.4) freshly supplemented with 1 mM ATP, 1 mM phenylmethylsulfonyl fluoride, and protease inhibitors (P8340; Sigma-Aldrich). After the lysate was clarified by

centrifugation at  $20,000 \times g$  for 10 min at  $4^{\circ}\text{C}$ , aliquots of the supernatant were snap-frozen in liquid nitrogen and stored at  $-80^{\circ}\text{C}$  until further use.

### Single-molecule motility assays

HiLyte647-labeled microtubules were polymerized from purified tubulin including 10% Hily647-labeled tubulin (Cytoskeleton) in BRB80 buffer (80 mM Pipes/KOH pH 6.8, 1 mM  $\text{MgCl}_2$ , and 1 mM EGTA) supplemented with 1 mM GTP and 2.5 mM  $\text{MgCl}_2$  at  $37^{\circ}\text{C}$  for 30 min. 20  $\mu\text{M}$  taxol in prewarmed BRB80 buffer was added and incubated at  $37^{\circ}\text{C}$  for additional 30 min to stabilize microtubules. Microtubules were stored in the dark at room temperature for further use.

A flow cell ( $\sim 10 \mu\text{l}$  volume) was assembled by attaching a clean #1.5 coverslip (Fisher Scientific) to a glass slide (Fisher Scientific) with two strips of double-sided tape. Polymerized microtubules were diluted in BRB80 buffer supplemented with 10  $\mu\text{M}$  taxol and then were infused into flow cells and incubated for 5 min at room temperature for nonspecific adsorption to the coverslips. Subsequently, blocking buffer [15 mg/ml BSA in P12 buffer (12 mM Pipes/KOH pH 6.8, 1 mM  $\text{MgCl}_2$ , and 1 mM EGTA)] was infused and incubated for 5 min. Finally, KIF6 cell lysate in the motility mixture [2 mM ATP, 0.4 mg/ml casein, 6 mg/ml BSA, 10  $\mu\text{M}$  taxol, and oxygen scavenging (1 mM DTT, 1 mM  $\text{MgCl}_2$ , 10 mM glucose, 0.2 mg/ml glucose oxidase, and 0.08 mg/ml catalase) in P12 buffer] was added to the flow cells. The flow-cell was sealed with molten paraffin wax. To examine the movement direction of dKif6 and mKif6, motility buffer containing the cell lysates of Kif6-mNG and KIF1A(1-393)-Halo<sup>JFX554</sup> was added into the flow cell and the flow cell was sealed and imaged.

Images were acquired by TIRF microscopy using an inverted microscope Ti-E/B equipped with the perfect focus system (Nikon), a  $100\times$  1.49 NA oil immersion TIRF objective (Nikon), three 20-mW diode lasers (488 nm, 561 nm, and 640 nm) and an electron-multiplying charge-coupled device detector (iXon X3DU897; Andor Technology). Image acquisition was controlled using Nikon Elements software and all assays were performed at room temperature. Images were acquired, at a rate of 1 frame every 3 sec for 3 min, for mKif6, or at a rate of 1 frame every 100 ms for 10 sec, for KIF1A.

Maximum-intensity projections were generated, and the kymographs were produced by drawing along tracks of motors (width= 3 pixels) using Fiji/ImageJ2. Motors frequently paused during motility events, and thus the velocity between pauses were analyzed. Velocity was defined as the distance on the x axis of the kymograph divided by the time on the y axis of the kymograph.

### **Ependymal cell culture**

LV walls from 3 or 4 mouse brains at P0 or P1 were collected and the suspended cells with trypsin-EDTA were cultured in DMEM with 10% FBS for 3 days on a laminin-coated flask. After shaking 2hr, the adherent cells were plated on poly-L-lysine and laminin-coated coverslips and differentiated into ciliated ependymal cells (ependymal cells) by serum starvation. ependymal cells were transfected with mKif6 (1-493)-mNG or mCherry-Kif6 constructs at 48hr before experiments using Lipofectamine 2000 (Invitrogen).

### **Live cell imaging**

For live imaging of Kif6 (1-493)-mNG, D5 ependymal cells were transfected with Kif6 (1-493)-mNG imaged at D7 for 5min in 0.2 fps, using Ti2E microscope with high content screening system (Nikon). To observe cilia beatings, ependymal cells were plated on the glass-bottom dish. Time-lapse images of DIC were collected for 2 sec in 47, 95 or 190 fps, using Ti2E microscope with high content screening system (Nikon). Ciliary tips were tracked by manual tracking of Fiji for images in Fig. 3H and 3K. Kymographs in Fig.3I were generated along the track of ciliary tip in 47fps for 200msec. The time of one beat (round-trip) of ciliary tip were measured in kymographs. Ciliary beating frequency (Hz) was calculated as how many beats per second. Immotile cilia, as showed in the bottom panel of Figure3I, was counted as 0.

### Western blotting

LV wall tissues were collected from 3 mice at P0, 4, 7, or 14. LV wall tissues or P45 testis tissue were lysed in PHEM buffer (50 mM PIPES, 50 mM HEPES, 1 mM EDTA, 2 mM MgSO<sub>4</sub>, 1% Triton X-100) with protease inhibitors, homogenized, and centrifuged for 1 hr at 14,000 rpm. The lysate supernatant was mixed with Laemmli Sample buffer (Bio-Rad) and 2-mercaptoethanol and boiled. Samples were separated by SDS-PAGE and transferred to Nitrocellulose membranes. The membranes were blocked with 2% BSA and probed with anti-Kif6 (1:1000, Proteintech, 17290-I-AP) or anti-GAPDH (1:1000, Cell Signaling Technology, #2118) antibodies. Detection was carried out using HRP-linked anti-Rabbit IgG (1:2000, Cell signaling Technology, #7074) and visualized using Pierce ECL substrate (Thermo Fisher).

### H&E staining and immunostaining

Mouse brains were fixed in 4% paraformaldehyde at 4°C for overnight. The fixed whole brains were paraffin-embedded and cut into 5µm sections for H&E staining. To measure cilia length, The fixed brains were sectioned in the coronal plane at 100 µm on a vibratome and immunostained. Whole-mount preparations of LV wall tissue were fixed with cold methanol for 10min and 4% paraformaldehyde for overnight at 4°C. Cultured ependymal cells were fixed with cold methanol for 3min and 4% paraformaldehyde for 10 min at RT. Whole-mount, ependymal cell, or vibratome sectioned samples were blocked with 10% goat serum in PBS for 30 min and incubated with primary antibodies for overnight at 4°C. Primary antibodies, which were anti-Kif6 (1:100, Proteintech, 17290-I-AP), anti-Arl13b (1:200, Proteintech, 17711-I-AP), anti-Acetylated Tubulin (1:200, Sigma, T7451), anti-gamma Tubulin (1:100, Abcam, ab11321), anti-beta Tubulin (1:100, Abcam, ab7287), anti-Centrin (1:50, Sigma, 04-1624), anti-FGFR1OP (1:100, Proteintech, 11343-1-AP), anti-Dnai1 (1:100, NeuroMab, 73-372), or anti-Tubulin [YL 1/2] (1:200, Abcam, ab6160), were detected with secondary antibodies conjugated to Alexa Fluorophores (Invitrogen). The apical surface of ependymal cells was imaged using a confocal laser scanning microscope LSM700 (Zeiss) or LSM980 Airyscan2 SR mode with joint Deconvolution (Nikon) for

super-resolution images. H&E or immune-stained tissue sections were imaged by BZ-X710 (KEYENCE).

### **Beads migration on LV wall**

Lateral side of LV walls were dissected from P12 mouse brain and pinned on a silicon plate with DMEM. Fluorescent microsphere (1 $\mu$ m) containing PBS was placed on the middle part of LV wall. The beads migration was recorded in 10 fps for 10sec by AXIO Zoom.V16 (Zeiss). Time projection images were created from 100 frames by Fiji software (Schindelin et al., 2012). Beads migration speed was calculated using the manual tracking plug-in of Fiji.

### **Electron microscopy**

P14 LV wall tissues were fixed using 3% glutaraldehyde with 2% paraformaldehyde for overnight. The tissues were post-fixed in 1% osmium tetroxide with 1% potassium ferrocyanide for 3hr. After en-bloc stain with 1% aqueous uranyl acetate for 1hr, ethanol-dehydrated tissues were displaced into acetone and embedded in an epoxy resin. Tissues were sectioned (80 nm thickness) with UltraCut Ultramicrotome (Leica). Images of the apical cell cortex of ependymal cells were obtained using Tecnai Transmission Electron Microscope (FEI).

### **Statistical analyses**

The violin plots were generated using GraphPad Prism 9 (GraphPad) Welch's t-test or Mann-Whitney U test was used to compare the means of two experimental groups using GraphPad Prism. Differences were considered statistically significant at  $P < 0.05$ . To determine the rotational BB orientation for a single ependymal cell (Fig.5E), a vector was drawn from the center of FOP dot to the center of the closest  $\gamma$ -tubulin dot in each cell, and more than 10 vectors were averaged. Vector angles were measured using Fiji and plotted on a circular diagram using the statistical software R (R Core Team, 2019). Mean resultant vector length (R bar) were calculated using the "circular" package (Lund

and Agostinelli, 2011) within the R statistical computing environment. For Fig.5I, Distribution of vector angles of cilia bundle on WT and *Kif6*<sup>pG555fs</sup> LV walls were compared using Watson's two-sample U2 test by R software.

## **Acknowledgements**

Kif6 mice was generated by Mia J. Konjikusic (University of California, San Francisco) and administrated by Elle C. Roberson (CU Anschutz, Colorado). Live imaging of cilia beatings and super-resolution imaging were performed at Microscopy and Imaging Facility at UT Austin (RRID# SCR\_021756).

## **Competing interests**

No competing interests declared.

## **Data availability**

All relevant data can be found within the article and its supplementary information.

## **Funding**

This work was supported by the NICHD (R01HD085901) and by the NHLBI (R01HL117164). MT was a research fellow of Japan Society for the Promotion of Science.

## References

1. Assimes, T.L., Hólm, H., Kathiresan, S., Reilly, M.P., Thorleifsson, G., Voight, B.F., Erdmann, J., Willenborg, C., Vaidya, D., Xie, C., et al. (2010). Lack of association between the Trp719Arg polymorphism in kinesin-like protein-6 and coronary artery disease in 19 case-control studies. *AJAm Coll Cardiol.* 56, 1552-1563.
2. Bare, L.A., Morrison, A.C., Rowland, C.M., Shiffman, D., Luke, M.M., Iakoubova, O.A., Kane, J.P., Malloy, M.J., Ellis, S.G., Pankow, J.S. et al. (2007). Five common gene variants identify elevated genetic risk for coronary heart disease. *Genet Med.* 9, 682-689.
3. Bottier, M., Thomas, K.A., Dutcher, S.K. and Bayly, P.V. (2019). How Does Cilium Length Affect Beating? *Biophys J.* 116, 1292-1304.
4. Brooks, E.R. and Wallingford, J.B. (2014). Multiciliated cells. *Curr Biol.* 24, R973-982.
5. Demonchy, R., Blisnick, T., Deprez, C., Toutirais, G., Loussert, C., Marande, W., Grellier, P., Bastin, P. and Kohl, L. (2009). Kinesin 9 family members perform separate functions in the trypanosome flagellum. *J Cell Biol.* 187, 615-622.
6. Gelfand, V.I., Le, Bot, N., Tuma, M.C. and Vernos, I. (2001). A Dominant Negative Approach for Functional Studies of the Kinesin II Complex. *Methods Mol Biol.* 164, 191-204.
7. Gennerich, A. and Vale, R.D. (2009). Walking the walk: how kinesin and dynein coordinate their steps. *Curr Opin Cell Biol.* 21, 59-67.
8. Gray, R.S., Gonzalez, R., Ackerman, S.D., Minowa, R., Griest, J.F., Bayrak, M.N., Troutwine, B., Canter, S., Monk, K.R., Sepich, D.S., et al. (2021). *Dev Biol.* 471, 18-33.

9. Hammond JW, Cai D, Blasius TL, Li Z, Jiang Y, Jih GT, Meyhofer E, and Verhey KJ. (2009). *PLoS Biol.* 7, e72.
10. Han L, Rao Q, Yang R, Wang Y, Chai P, Xiong Y, and Zhang K. (2022). *Nat Struct Mol Biol.* 5, 472-82.
11. Ishikawa, T. (2017). Axoneme Structure from Motile Cilia. *Cold Spring Harb Perspect Biol.* 9, a028076.
12. Konjikusic, M.J., Yeetong, P., Boswell, C.W., Lee, C., Roberson, E.C., Ittiwut, R., Suphapeetiporn, K., Ciruna, B., Gurnett, C.A., Wallingford, J.B., et al. (2018). Mutations in Kinesin family member 6 reveal specific role in ependymal cell ciliogenesis and human neurological development. *PLoS Genet.* 14, e1007817.
13. Konjikusic MJ, Gray RS, and Wallingford JB. (2021). The developmental biology of kinesins. *Dev Biol.* 469, 26-36.
14. Konjikusic, M.J., Lee, C., Yue, Y., Shrestha, B.D., Nguimtsop, A.M., Horani, A., Brody, S., Prakash, V.N., Gray, R.S., Verhey, K.J. and Wallingford, J.B. (2023). Kif9 is an active kinesin motor required for ciliary beating and proximodistal patterning of motile axonemes. *J Cell Sci.* 136, jcs259535.
15. Kunitomo K, Yamazaki Y, Nishida T, Shinohara K, Ishikawa H, Hasegawa T, Okanoue T, Hamada H, Noda T, Tamura A, et al. (2012). Coordinated ciliary beating requires Odf2-mediated polarization of basal bodies via basal feet. *Cell.* 148, 189-200.
16. Lechtreck, K.F. and Witman, G.B. (2007). Chlamydomonas reinhardtii hydin is a central pair protein required for flagellar motility. *J Cell Biol.* 176, 473-482.

17. Li, Y., Chen, Z. and Song, H. (2018). Association between KIF6 rs20455 polymorphism and the risk of coronary heart disease (CHD): a pooled analysis of 50 individual studies including 40,059 cases and 64,032 controls. *Lipids Health Dis.* 17, 4.
18. Mahuzier, A., Shihavuddin, A., Fournier, C., Lansade, P., Faucourt, M., Menezes, N., Meunier, A., Garfa-Traoré, M., Carlier, M.F., Voituriez, R. et al. (2018). Ependymal cilia beating induces an actin network to protect centrioles against shear stress. *Nat Commun.* 9, 2279.
19. Ma, M., Stoyanova, M., Rademacher, G., Dutcher, S.K., Brown, A. and Zhang, R. (2019). Structure of the Decorated Ciliary Doublet Microtubule. *Cell.* 179, 909-922.e12.
20. McCafferty, C.L., Papoulas, O., Lee, C., Bui, K.H., Taylor, D.W., Marcotte, E.M., and Wallingford, J.B. (2023). An amino acid-resolution interactome for motile cilia illuminates the structure and function of ciliopathy protein complexes. *bioRxiv* doi: 10.1101/2023.07.09.548259.
21. Mirzadeh, Z., Han, Y.G., Soriano-Navarro, M., García-Verdugo, J.M. and Alvarez-Buylla, A. (2010). Cilia Organize Ependymal Planar Polarity. *J Neurosci.* 30, 2600-2610.
22. Miyata, H., Shimada, K., Morohoshi, A., Oura, S., Matsumura, T., Xu, Z., Oyama, Y. and Ikawa, M. (2020). Testis-enriched kinesin KIF9 is important for progressive motility in mouse spermatozoa. *FASEB J.* 34, 5389-5400.
23. Ohata, S. and Alvarez-Buylla, A. (2016). Planar Organization of Multiciliated Ependymal (E1) Cells in the Brain Ventricular Epithelium. *Trends Neurosci.* 39, 543-551.

24. Piddini, E., Schmid, J.A., de Martin, R. and Dotti, C.G. (2001). The Ras-like GTPase Gem is involved in cell shape remodelling and interacts with the novel kinesin-like protein KIF9. *EMBO J.* 20, 4076-4087.
25. Prevo, B., Scholey, J.M. and Peterman, E.J.G. (2017). Intraflagellar transport: mechanisms of motor action, cooperation, and cargo delivery. *FEBS J.* 284, 2905-2931.
26. Roberson EC, Tran NK, Konjikusic MJ, Fitch RD, Gray RS, and Wallingford JB. (2020). A comparative study of the turnover of multiciliated cells in the mouse trachea, oviduct, and brain *Dev Dyn.* 249, 898-905.
27. Ruiz-Ramos D, Hernández-Díaz Y, Tovilla-Zárate CA, Juárez-Rojop I, López-Narváez ML, González-Castro TB, Torres-Hernández ME, and Baños-González MA. (2015). The Trp719Arg polymorphism of the KIF6 gene and coronary heart disease risk: systematic review and meta-analysis. *Hereditas.* 152, 3.
28. Shiffman, D., O'Meara, E.S., Bare, L.A., Rowland, C.M., Louie, J.Z., Arellano, A.R., Lumley, T., Rice, K., Iakoubova, O., Luke, M.M., et al. (2008)-a. Association of gene variants with incident myocardial infarction in the Cardiovascular Health Study. *Arterioscler Thromb Vasc Biol.* 28, 173-179.
29. Shiffman, D., Chasman, D.I., Zee, R.Y., Iakoubova, O.A., Louie, J.Z., Devlin, J.J. and Ridker, P.M. (2008)-b. A kinesin family member 6 variant is associated with coronary heart disease in the Women's Health Study. *J Am Coll Cardiol.* 51, 444-448.
30. Spassky, N. and Meunier, A. (2017). The development and functions of multiciliated epithelia. *Nat Rev Mol Cell Biol.* 18, 423-436.

31. Soppina V, Norris SR, Dizaji AS, Kortus M, Veatch S, Peckham M, and Verhey KJ. (2014). Dimerization of mammalian kinesin-3 motors results in superprocessive motion. *Proc Natl Acad Sci U S A.* 111, 5562-7.
32. Takagishi, M., Esaki, N., Takahashi, K. and Takahashi, M. (2020). Cytoplasmic Dynein Functions in Planar Polarization of Basal Bodies within Ciliated Cells. *iScience.* 23, 101213.
33. Verhey, K.J. and Hammond, J.W. (2009). Traffic control: regulation of kinesin motors. *Nat Rev Mol Cell Biol.* 10, 765-777.
34. Vladar, E.K., Bayly, R.D., Sangoram, A.M., Scott, M.P. and Axelrod, J.D. (2012). Microtubules Enable the Planar Cell Polarity of Airway Cilia. *Curr Biol.* 22, 2203-2212.
35. Werner, M.E., Hwang, P., Huisman, F., Taborek, P., Yu, C.C. and Mitchell, B.J. (2011). Actin and microtubules drive differential aspects of planar cell polarity in multiciliated cells. *J Cell Biol.* 195, 19-26.
36. Wickstead, B., Gull, K. and Richards, T.A. (2010). Patterns of kinesin evolution reveal a complex ancestral eukaryote with a multifunctional cytoskeleton. *BMC Evol Biol.* 10, 110.
37. Yokoyama, R., O'toole, E., Ghosh, S. and Mitchell, D.R. (2004). Regulation of flagellar dynein activity by a central pair kinesin. *Proc Natl Acad Sci USA.* 101, 17398-403.

Figures

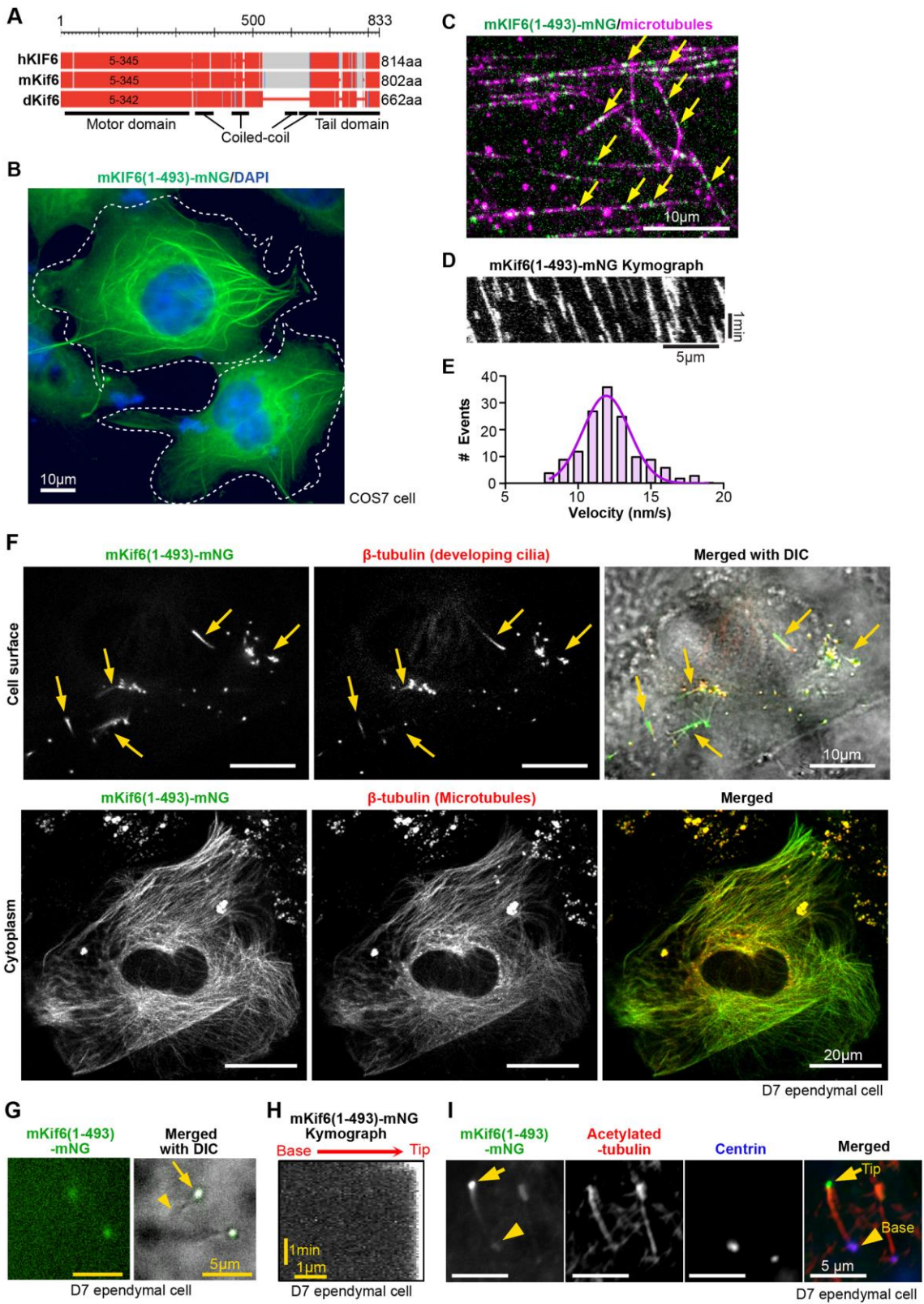


**Fig. 1. Kif6 is an active motor that localizes to cytoplasmic and ciliary microtubules**

- (A) Schematic representation of human, mouse, and danio Kif6 proteins. The predicted motor domain is 5-345aa in hKIF6, 5-345aa in mKif6, and 5-342aa in dKif6. Red regions are highly conserved positions with human, mouse, and danio.
- (B) Representative image of mNeongreen (mNG)-tagged mKif6(1-493) expressed in COS-7 cells. White dashed line indicates the outline of a transfected cell. Blue, DAPI stain.
- (C) Representative still image from single-molecule motility assay of mKif6(1-493)-mNG molecules (green) on taxol-stabilized microtubules (magenta). Arrows indicate individual mKif6(1-493)-mNG molecules on microtubules.
- (D) Kymograph of mKif6(1-493)-mNG movement from the single-molecule motility assay shown in (C). Time is on the y-axis and distance is on the x-axis.
- (E) The velocities of individual mKif6(1-493)-mNG were determined from kymographs and plotted as a histogram for the population. The curve was fit with a normal distribution. Velocity is described as mean  $\pm$  std. dev. n=143 motility events analyzed across three independent experiments.
- (F) mKif6(1-493)-mNG expressed in cultured developing ependymal cell at D7. Upper panels show mKif6(1-493)-mNG (green), immunostained- $\beta$ -tubulin (red) and merged image with DIC on cell surface to see cilia (arrows). Lower panels show mKif6(1-493)-mNG and  $\beta$ -tubulin (red) in the same cell at the cytoplasmic plane.
- (G) Still frame from live imaging of mKif6 (1-493)-mNG in a developing short cilia of a D7 ependymal cell. Arrow indicates ciliary tip. Arrowhead indicates ciliary base. See supplemental movie 2.

(H) Kymograph of mKif6 (1-493)-mNG movement along cilia in the live imaging shown in (G).

(I) mKif6(1-493)-mNG expressing ependymal cells were immunostained with acetylated-tubulin (red, cilia marker) and Centrin (magenta, ciliary base). Arrow indicates ciliary tip. Arrowhead indicates ciliary base.

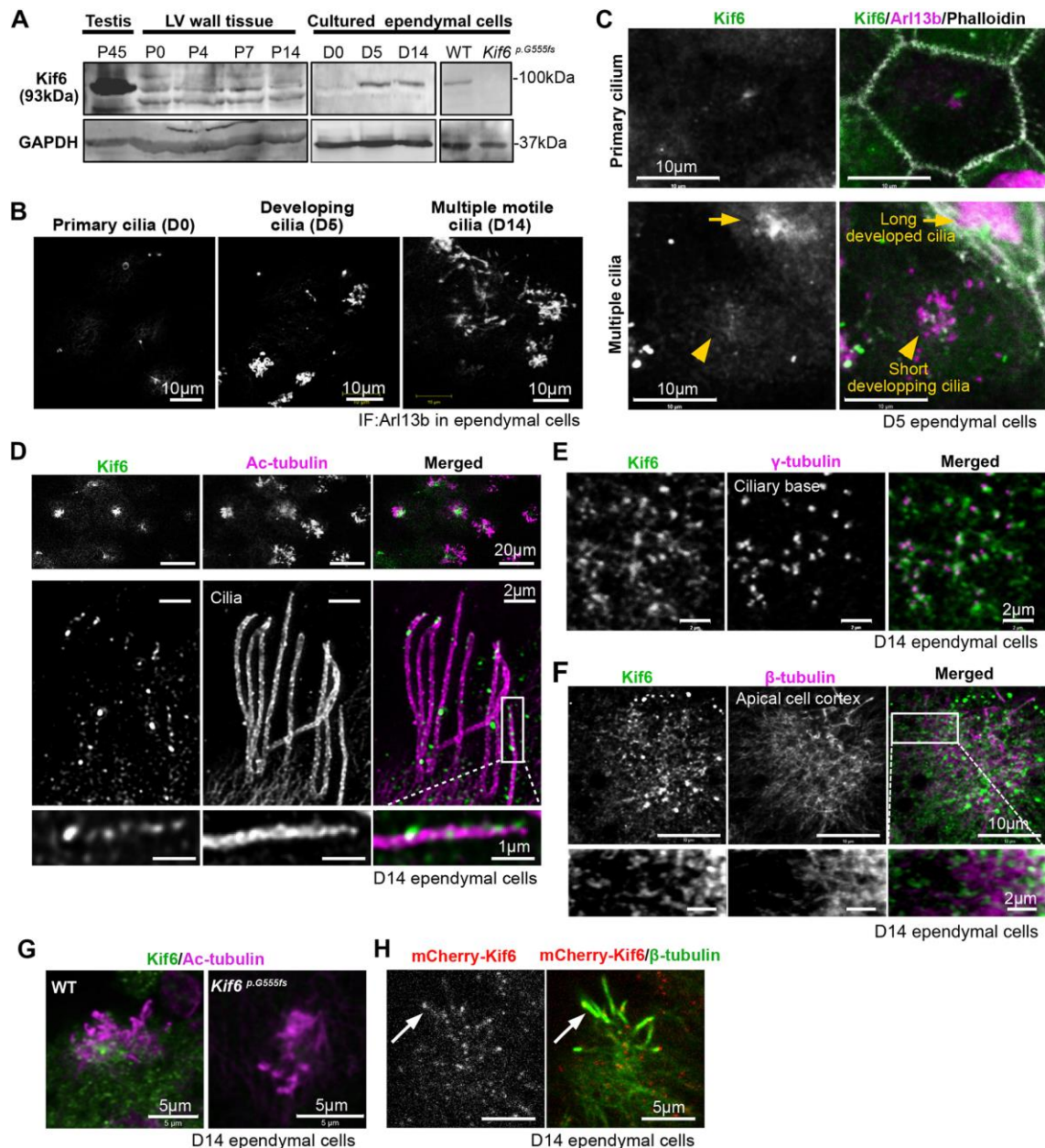


**Fig. 2. Kif6 localizes to the cytoplasm and cilia of multiciliated ependymal cells**

- (A) Western blot analysis with anti-Kif6 or anti-GAPDH in P45 mouse testis tissue, P0, 4, 7, or 14 mouse LV wall tissues, or D0, 5, or 14 cultured ependymal cell lysates. Right panels show D14 ependymal cell lysate from WT or *Kif6*<sup>p.G555fs</sup> mice.
- (B) Representative image of cilia formation in cultured ependymal cells at D0, 5, or 14. ependymal cells were immunostained with anti-Arl13b.

- (C) Immunostaining with anti-Kif6 (green), anti-Arl13b (magenta, as a cilia marker), and Phalloidin (gray, as a cell border marker) in differentiating ependymal cells at D5. Upper panels show primary ciliated precursor cell. Lower panels show multiple ciliated differentiating ependymal cells.
- (D) Super-resolution image of immunostaining with anti-Kif6 (green) and anti-Acetylate (Ac)-tubulin (magenta) in differentiated ependymal cell cilia at D14. Top panels show Kif6 expression in the differentiated ependymal cells at low magnification. Middle panels show representative ependymal cilia in one ependymal cell. Boxed area is enlarged in the bottom panels.
- (E) Immunostaining with anti-Kif6 (green) and anti- $\gamma$ -tubulin (magenta, as a BF marker) at the cytoplasmic ciliary base.
- (F) Immunostaining with anti-Kif6 (green) and anti- $\beta$ -tubulin (magenta, as a microtubules marker) at the apical cell cortex.
- (G) Immunostaining with anti-Kif6 (green) at cilia and ciliary base in D14 ependymal cell from WT or *Kif6*<sup>p.G555fs</sup> as negative control.
- (H) mCherry-Kif6 (white in left panel, red in right panel) expressing cells are immunostained with anti- $\beta$ -tubulin (green). Arrow indicates mCherry-Kif6 localization at cilia.

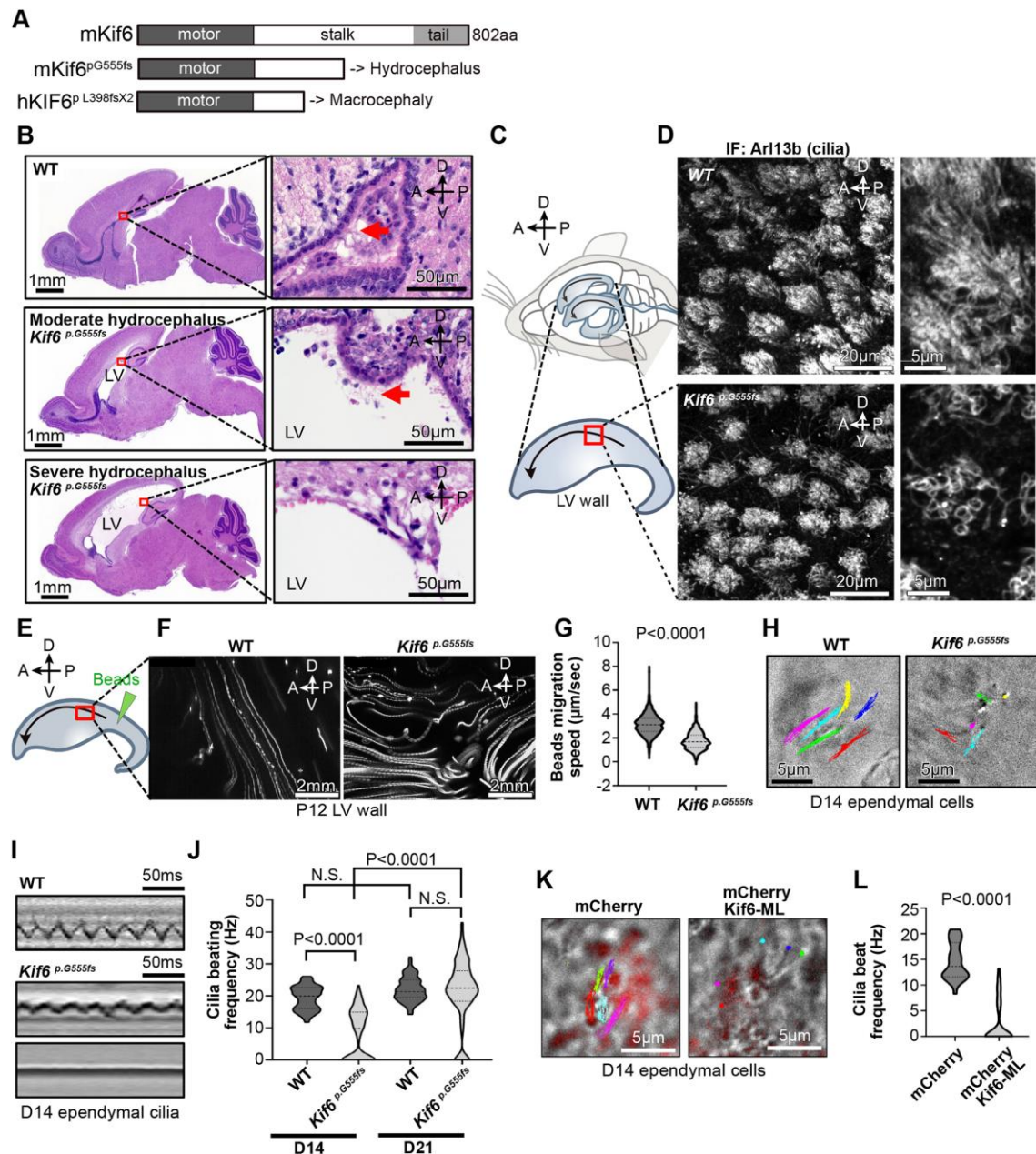


**Fig. 3. Kif6 regulates cilia motility in ependymal cells**

(A) Schematic representation of mouse Kif6 WT, mouse Kif6<sup>p.G555fs</sup> mutant, which resulted in hydrocephalus in mice, or human KIF6<sup>p.L398fsX2</sup> mutant, which causes macrocephaly in a patient, proteins.

(B) H&E-stained sagittal section in WT or *Kif6*<sup>p.G555fs</sup> mice brains at P14. Red boxes indicate the wall of Lateral ventricle (LV) expanded in the right panels. Arrows

represent ependymal cilia. LV wall in *Kif6<sup>p.G555fs</sup>* mice with severe hydrocephalus is broken and lose ependymal cells.

- (C) Illustration of mouse brain ventricles and dissected LV wall. Arrows represent CSF flow direction. CSF is produced at the choroid plexus in the posterior region within LV, and outflows through the Foremen of Monro at the anterior-ventral region of the LV, towards the third ventricle. The illustration below represents the surface of a dissected right distal LV wall. A, anterior, P, posterior, D, dorsal, V, ventral sides of the brain.
- (D) Fluorescence microscopy images of the red boxed area in (C) are shown to see the surface cilia formation in P14 WT or *Kif6<sup>p.G555fs</sup>*. LV wall tissues were whole-mount immunostained with anti-Arl13b as a cilia marker.
- (E) Representation of beads migration assay on the surface of LV wall tissue at P12. Fluorescent microbeads are placed on the green arrowhead region and migrate toward the anterior-ventral side along the CSF flow (arrow).
- (F) Time projections of beads migration on WT or *Kif6<sup>p.G555fs</sup>* LV wall at the red boxed area shown in (E). 100 frames are overlaid from the movie in 10fps. See supplemental movie 3-4.
- (G) Beads migration speeds are quantified in P12 WT or *Kif6<sup>p.G555fs</sup>* LV wall. The violin plots show distribution with median and quartile in WT (Median=3.11, n=517frames of 53 beads on 3 LV walls) or *Kif6<sup>p.G555fs</sup>* (Median=1.67, n=513frames of 58 beads on 3 LV walls). P-value was determined with the Mann–Whitney test.
- (H) Movement tracks of cilia for 0.3 sec in the cultured ependymal cells from WT or *Kif6<sup>p.G555fs</sup>*, at D14. See supplemental movie 5-7.
- (I) Representative kymographs of cilia in D14 cultured WT (top panel) or *Kif6<sup>p.G555fs</sup>* ependymal cells. *Kif6<sup>p.G555fs</sup>* cilia have slow motility (middle panel) or no motility (bottom panel).
- (J) Graph represents cilia beating frequency (Hz) in D14 cultured WT or *Kif6<sup>p.G555fs</sup>* ependymal cells. The truncated violin plots show distribution with median and

quartile in D14 WT (Median=19.9, n=118 cilia from 3 experiments), D14 *Kif6*<sup>p.G555fs</sup> (Median=9.79, n=118 cilia from 3 experiments), D22 WT (Median=20.82, n=98 cilia from 2 experiments), or D14 *Kif6*<sup>p.G555fs</sup> (Median=23.08, n=98 cilia from 2 experiments). P-values were determined with the Mann–Whitney test.

- (K) Movement tracks of cilia for 0.23sec in D14 cultured ependymal cell transfected with mCherry or mCherry-Kif6 motor less (ML) as a dominant negative form of Kif6. See supplemental movie 8-9.
- (L) Graph indicates cilia beating frequency (Hz) in mCherry or mCherry-Kif6 ML expressing ependymal cells. The truncated violin plots show distribution with median and quartile in mCherry (Median=13.62, n=32 cilia from 3 experiments) or mCherry-Kif6 ML (Median=0.000, n=32 cilia from 3 experiments). P-value was determined with the Mann–Whitney test.

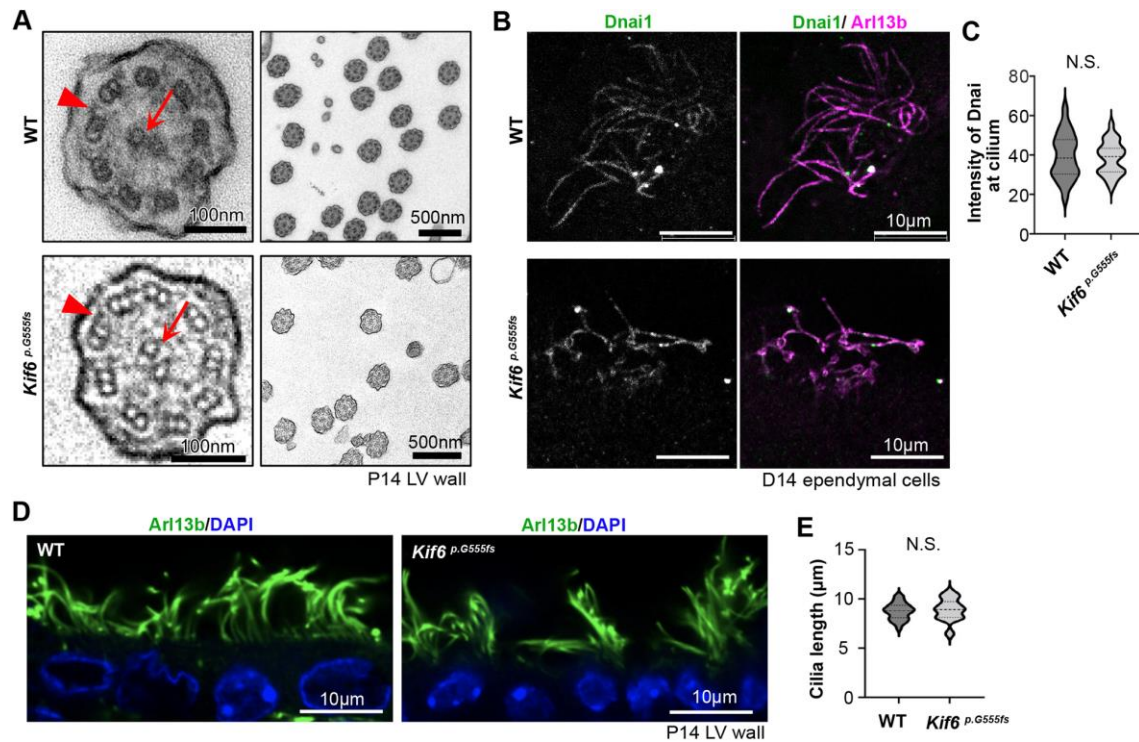


**Fig. 4. Ependymal cilia in *Kif6*<sup>p.G555fs</sup> display relatively normal axoneme ultrastructure**

- (A) Representative TEM images of ependymal cilia at P14 WT or *Kif6*<sup>p.G555fs</sup> LV wall. Arrows indicate central pair of microtubules. Arrowheads indicate outer dynein arm.
- (B) WT or *Kif6*<sup>p.G555fs</sup> ependymal cells at D14 were immunostained with anti-Dnai1 (green, outer dynein arm marker) and anti-Arl13b (magenta).
- (C) Quantification of Dnai1 intensity at cilia. Mean intensity of Dnai1 were normalized by Arl13b intensity at cilia. The violin plots show distribution with median and quartile in D14 WT (Median=38.53, n=48 cilia from 3 experiments) or D14 *Kif6*<sup>p.G555fs</sup> (Median=39.25, n=48 cilium from 3 experiments). P-value (0.796) was determined with the Mann Whitney test.

- (D) Cross section of ependymal cells in the middle lateral side of LV wall. Vibratome section from P14 WT or *Kif6*<sup>p.G555fs</sup> brain are immunostained with anti-Arl13b (green) and DAPI (blue).
- (E) Graph represents cilia length in WT or *Kif6*<sup>p.G555fs</sup> LV wall. The violin plots show distribution with median and quartile in P14 WT (Median=8.821, n=49 cilia from 3 mice) or P14 *Kif6*<sup>p.G555fs</sup> (Median=8.928, n=49 cilia from 3 mice). P-value (0.4341) was determined with the Welch's test.

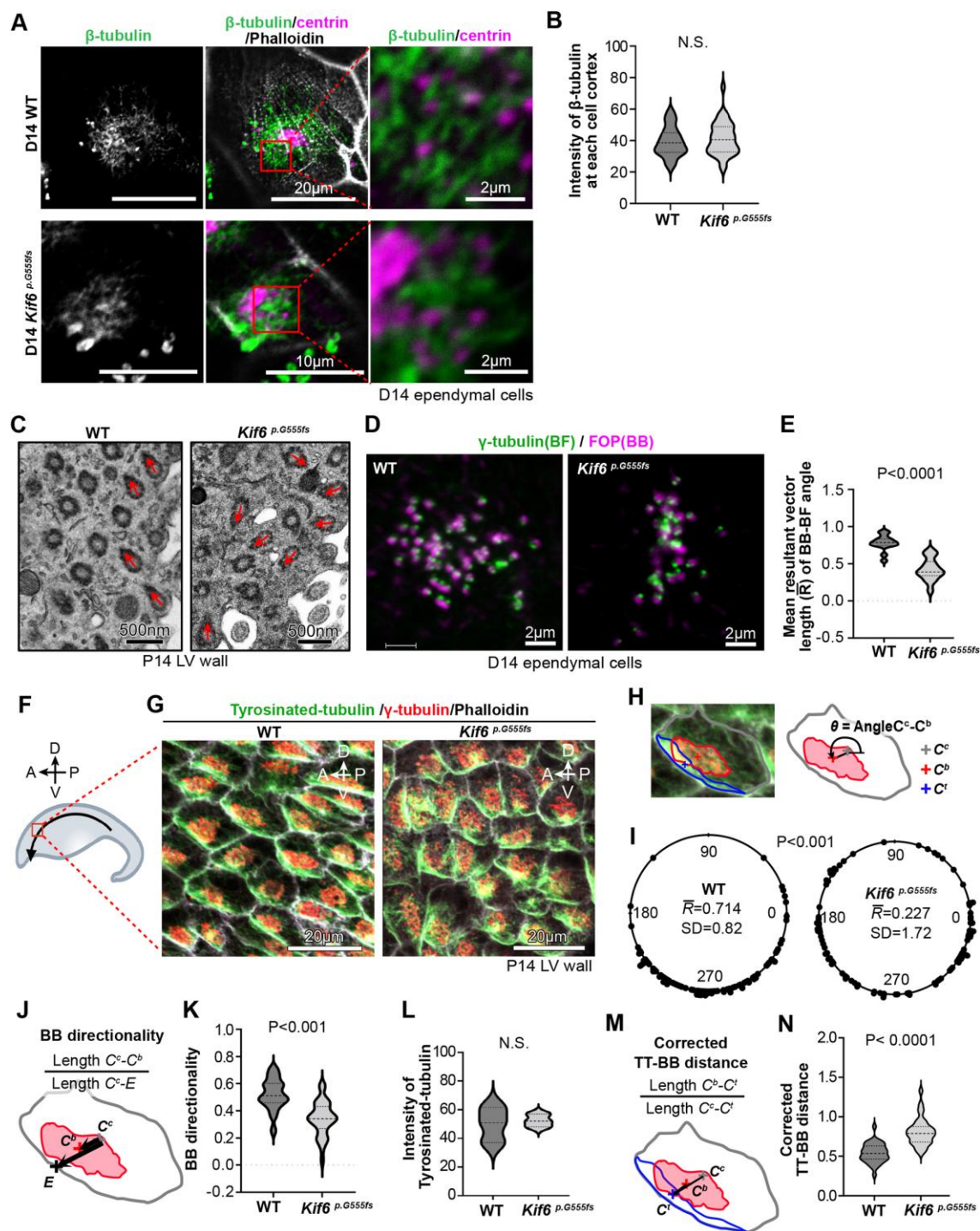


**Fig. 5. *Kif6*<sup>p.G555fs</sup> is required for planar polarization of ependymal cells**

(A) Representative images of apical microtubules at ciliary base in D14 WT or *Kif6*<sup>p.G555fs</sup> ependymal cells. WT or *Kif6*<sup>p.G555fs</sup> cells are immunostained with anti- $\beta$ -tubulin (green), anti-centrin (magenta), and Phalloidin (gray). Red boxes show microtubules connecting BBs, expanded in the right panels.

- (B) Graph represents intensity of  $\beta$ -tubulin at apical cell cortex. The violin plots show distribution with median and quartile in P14 WT (Median=38.52, n=37 cells from 3 LV walls) or P14 *Kif6*<sup>p.G555fs</sup> (Median=40.62, n=37 cells from 3 LV walls). P-value (0.36) was determined with the Welch's test.
- (C) TEM images of ciliary base in ependymal cell from P14 WT or *Kif6*<sup>p.G555fs</sup> LV wall. Arrows indicate vectors from BB to BF.
- (D) Representative immunostaining images of  $\gamma$ -tubulin (green, as a BF marker) and FOP (magenta, as a BB marker) in D14 WT or *Kif6*<sup>p.G555fs</sup> ependymal cells.
- (E) Graph represents mean resultant vector length (R bar) of BB-BF angle that are measured in the immunostaining images as shown in (D). The violin plots show distribution with median and quartile in D14 WT (Median=0.79, n=15 cells from 2 experiments) or D14 *Kif6*<sup>p.G555fs</sup> (Median=0.39, n=15 cells from 2 experiments). P-value was determined with the Welch's test.
- (F) Representation of the measurement area to observe translational polarity in LV wall tissue at P14. Whole mount-immunostained LV walls were observed at anterior area (red box) of LV wall. Arrow indicates direction of CSF flow.
- (G) Representative images of whole-mount immunostaining with anti-Tyrosinated-tubulin (green), anti- $\gamma$ -tubulin (red), and Phalloidin (gray) in the anterior area of P14 WT or *Kif6*<sup>p.G555fs</sup> LV walls.
- (H) Illustration represents the measurement of BB clustering position in apical cell cortex of ependymal cell. Vector angles ( $\theta$ ) were calculated from the center of the cell to the center of the multicilia bundle base (BB clustering), which is aggregated region of  $\gamma$ -tubulin dots.
- (I) Vector angles ( $\theta$ ) were plotted on circular diagram in P14 WT or *Kif6*<sup>p.G555fs</sup> LV walls. The mean resultant vector length (R bar) and SD of  $\theta$  were calculated in WT (R bar=0.714, n=100 cells from 3 mice) or *Kif6*<sup>p.G555fs</sup> (R bar=0.227, n=100 cells from 3 mice). P-value was determined with Watson's two-sample test.

- (J) Illustration represents the measurement of the directionality of BB clustering to cell border. The length between the center of cell and the center of BB clustering ( $C^c-C^b$ ) were divided by the length between center of cell and cell edge ( $C^c-E$ ), as “BB directionality”.
- (K) Graph represents “BB directionality” in P14 WT or *Kif6*<sup>p.G555fs</sup> LV walls, measured as shown in (J). The violin plots show distribution with median and quartile in P14 WT (Median=0.51, n=56 cells from 3 mice) or P14 *Kif6*<sup>p.G555fs</sup> (Median=0.34, n=56 cells from 3 mice). P-value was determined with the Welch’s test.
- (L) Graph represents the intensity of Tyrosinated-tubulin at apical cell cortex as shown in (G). The violin plots show distribution with median and quartile in P14 WT (Median=50.93, n=3 mice) or P14 *Kif6*<sup>p.G555fs</sup> (Median=52.01, n=3 mice). P-value (0.7717) was determined with Welch’s test.
- (M) Illustration represents the measurement of the distance between the polarized tyrosinated-tubulin and BB clustering. The length between the center of BB clustering and the center of the asymmetrically accumulated tyrosinated-tubulin area (the polarized tyrosinated-tubulin) ( $C^b-C^t$ ) were divided by the length between the center of cell and the center of the polarized tyrosinated-tubulin ( $C^c-C^t$ ), as “Corrected TT-BB distance”.
- (N) Graph represents “Corrected TT-BB distance” in P14 WT or *Kif6*<sup>p.G555fs</sup> LV walls, measured as shown in (M). The violin plots show distribution with median and quartile in P14 WT (Median=0.537, n=34 cells from 3 mice) or P14 *Kif6*<sup>p.G555fs</sup> (Median=0.787, n=34 cells from 3 mice). P-value was determined with the Mann Whitney test.

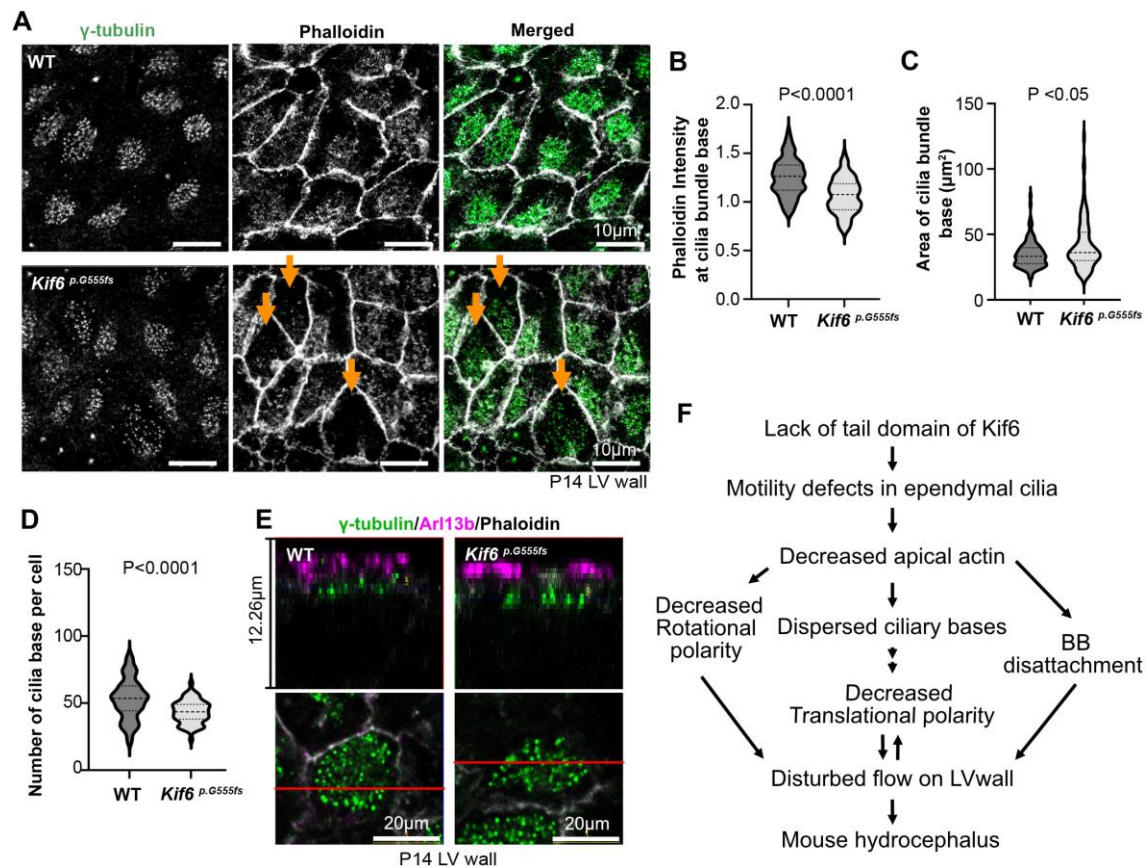


**Fig. 6. *Kif6*<sup>p.G555fs</sup> decreases apical actin and BB stability**

- (A) Representative images of whole mount immunostaining with  $\gamma$ -tubulin (green) and Phalloidin (gray) in the anterior area of P14 WT or *Kif6*<sup>p.G555fs</sup> LV walls. Arrows indicates the cells with decreased phalloidin and dispersed ciliary bases.
- (B) Graph represents Phalloidin intensity at cilia bundle base. The intensity of phalloidin at  $\gamma$ -tubulin dots area were divided by the intensity of Phalloidin at the apical cell cortex. The violin plots show distribution with median and quartile in P14 WT (Median=1.26, n=100 cells from 3 mice) or P14 *Kif6*<sup>p.G555fs</sup> (Median=1.08, n=99 cells from 3 mice). P-value was determined with the Welch's test.
- (C) Graph represents the spreading area of  $\gamma$ -tubulin dots as the area of cilia bundle bases. The violin plots show distribution with median and quartile in P14 WT (Median=33.21, n=100 cells from 3 mice) or P14 *Kif6*<sup>p.G555fs</sup> (Median=36.08, n=101 cells from 3 mice). P-value (0.0162) was determined with the Mann Whitney test.

- (D) Graph represents the number of  $\gamma$ -tubulin dots in apical cell cortex as the number of cilia base per cell. The violin plots show distribution with median and quartile in P14 WT (Median=53.50, n=60 cells from 3 mice) or P14 *Kif6*<sup>p.G555fs</sup> (Median=43.5, n=60 cells from 3 mice). P-value was determined with the Mann Whitney test.
- (E) Representative confocal microscopy images of whole mount immunostaining with  $\gamma$ -tubulin (green), Arl13b (magenta), and Phalloidin (gray) in P14 WT or *Kif6*<sup>p.G555fs</sup> LV walls. Upper panels show cross sections of ependymal cell shown in lower panels at red line.
- (F) Effects of cilia disfunction in *Kif6*<sup>p.G555fs</sup> ependymal cells on mouse LV wall. Lack of tail domain of Kif6 (*Kif6*<sup>p.G555fs</sup>) causes motility defects in ependymal cells during brain development. Motility defects in ependymal cilia reduce apical actin network formation. Decreased apical actin results in de-stabilization of ciliary base, leading to decreased rotational polarity, dispersed ciliary bases, and BB dis-attachment, which in turn contributes to the disturbed flow on LV wall and mouse hydrocephalus.

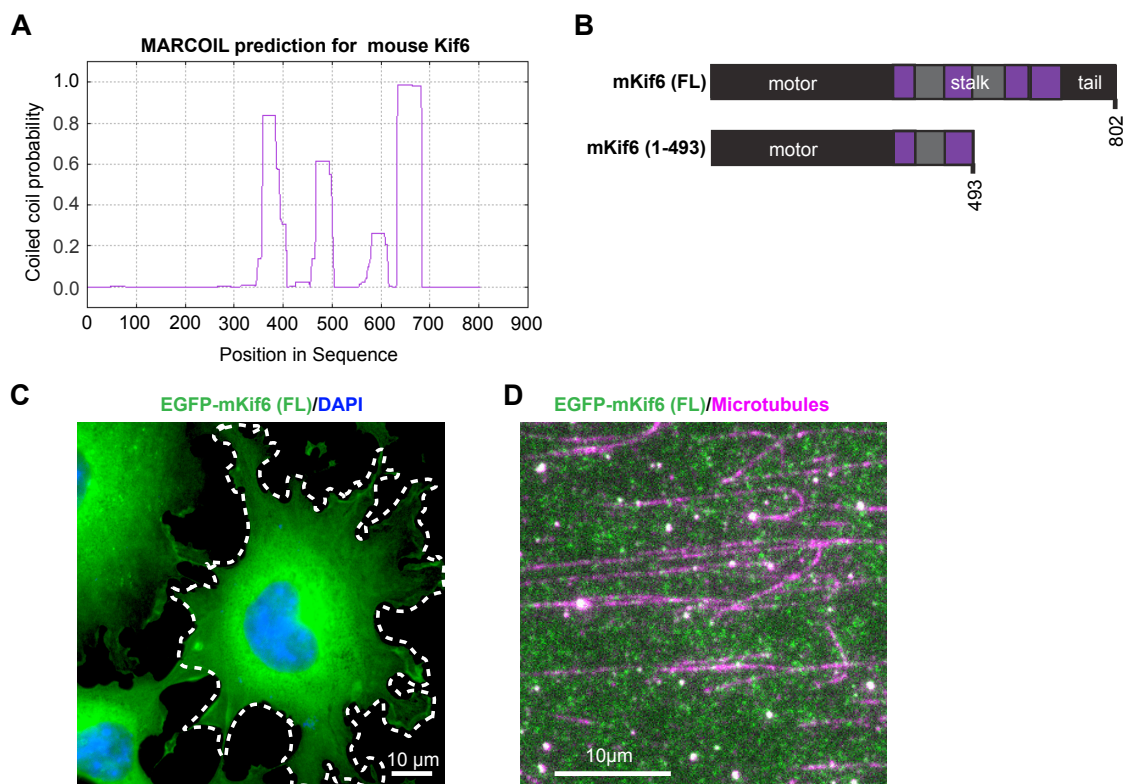


**Fig. S1. Full-length of Kif6 is regulated by autoinhibition, related to Figure1.**

(A) Coiled-coil predictions of mouse KIF6 using Marcoil prediction software (Delorenzi and Speed. 2002. Bioinformatics).

(B) Schematic of the domain composition of full-length and truncated active proteins.

(C) Representative images of mNG-tagged full-length mKIF6 expressed in COS-7 cells. White dashed lines indicate the outline of a transfected cell. Blue, DAPI stain. Scale bar, 10  $\mu$ m.

(D) Representative still images from single-molecule motility assays of mKif6(1-493)-mNG on taxol-stabilized microtubules (magenta). Scale bar, 10  $\mu$ m.

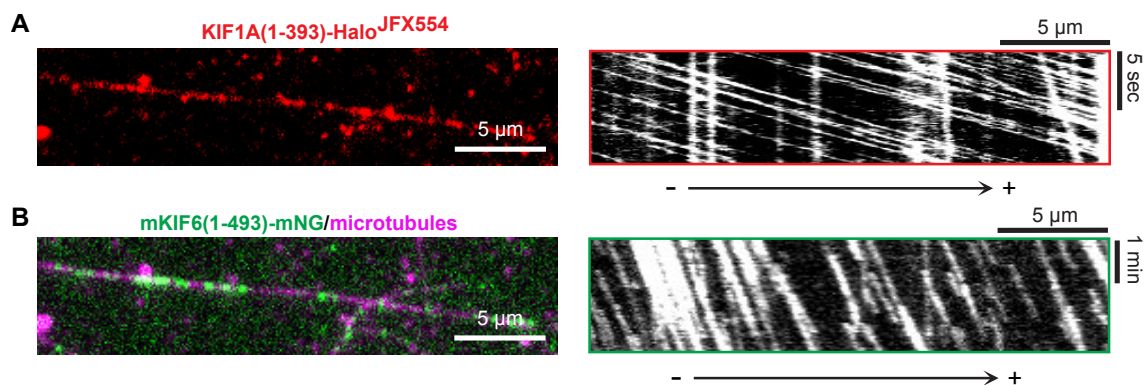


**Fig. S2. mKif6(1-493)-mNG moved in the same direction as KIF1A, related to Fig. 1.**

(A) Left, the representative still images from movies of KIF1A(1-393)-LZ-Halo<sup>JFX554</sup> (red). Right, the representative kymograph of KIF1A(1-393)-LZ-HaloJFX554. Time is on the y-axis (scale bar, 5 s) and distance is on the x-axis (scale bar, 5 μm).

(B) Left, mKIF6 (1-493)-mNG (green) along taxol-stabilized microtubules (magenta). Right, the kymograph of mKIF6 (1-493)-mNG at the same microtubules as shown in (A). Time is on the y-axis (scale bar, 5 s) and distance is on the x-axis (scale bar, 5 μm).

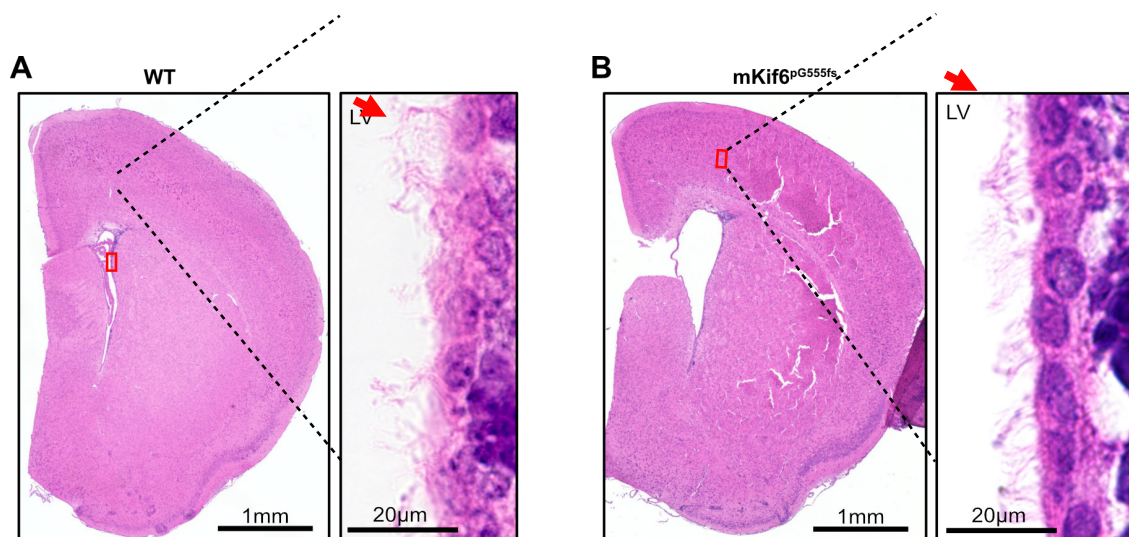


**Fig. S3. Ependymal cells on LV wall in P14 WT or in *Kif6<sup>p.G555fs</sup>* mice, related to Fig. 3.**

(A, B) H&E-stained coronal section in WT (A) or *Kif6<sup>p.G555fs</sup>* (B) mice brains at P14. Red boxes indicate the wall of Lateral ventricle (LV) expanded in the right panels. Arrows represent ependymal cilia.

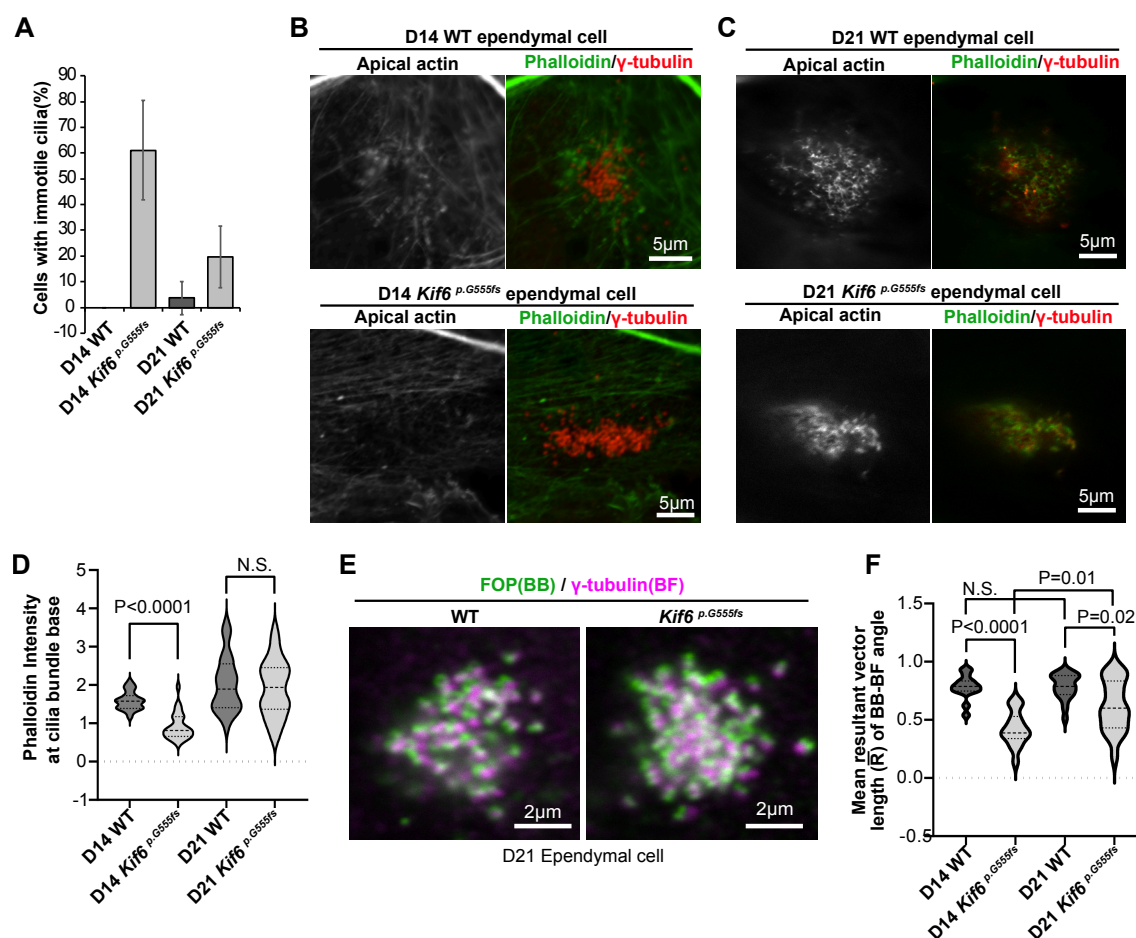


**Fig. S4. Apical actin and rotational polarity in cultured ependymal cells, related to Fig. 3 and 6.**

(A) Graph represents the percentage of cells with immotile cilia. The bar graph shows average and standard deviation of three different experiments in D14 WT (0%), D14 *Kif6*<sup>p.G555fs</sup> (61.1% ± 19.2), D21 WT (3.7% ± 6.4) or D21 *Kif6*<sup>p.G555fs</sup> (19.6% ± 12.0) ependymal cells.

(B) Representative images of immunostaining with Phalloidin (green) and γ-tubulin (red) in D14 WT (upper panels) or *Kif6*<sup>p.G555fs</sup> (lower panels) ependymal cell.

(C) Representative images of immunostaining with Phalloidin (green) and γ-tubulin (red) in D21 WT (upper panels) or *Kif6*<sup>p.G555fs</sup> (lower panels) ependymal cell.

(D) Graph represents Phalloidin intensity at cilia bundle base. The intensity of phalloidin at γ-tubulin dots area were divided by the intensity of Phalloidin at all area of apical cell cortex.

The violin plots show distribution with median and quartile in D14 WT (Median=1.579, n=27 cells from three different experiments), P14 *Kif6*<sup>p.G555fs</sup>

(Median=0.811, n=27 cells from three different experiments), D21 WT

(Median=1.892, n=27 cells from three different experiments), or P14 *Kif6*<sup>p.G555fs</sup>

(Median=1.939, n=27 cells from three different experiments). P-value was determined with the Mann Whitney test.

(E) Representative images of immunostaining with FOP (green) and  $\gamma$ -tubulin (magenta) in D21 WT (left panel) or *Kif6<sup>p.G555fs</sup>* (right panel) ependymal cell.

(F) Graph represents mean resultant vector length (R bar) of BB-BF angle that are measured in the immunostaining images as shown in Figure 5D and Figure S6D. The violin plots show distribution with median and quartile in D14 WT (Median=0.79, n=15 cells from two experiments), D14 *Kif6<sup>p.G555fs</sup>* (Median=0.39, n=15 cells from two experiments), D21 WT (Median=0.79, n=20 cells from three experiments), or D21 *Kif6<sup>p.G555fs</sup>* (Median=0.60, n=20 cells from three experiments). P-value was determined with the Mann Whitney test.

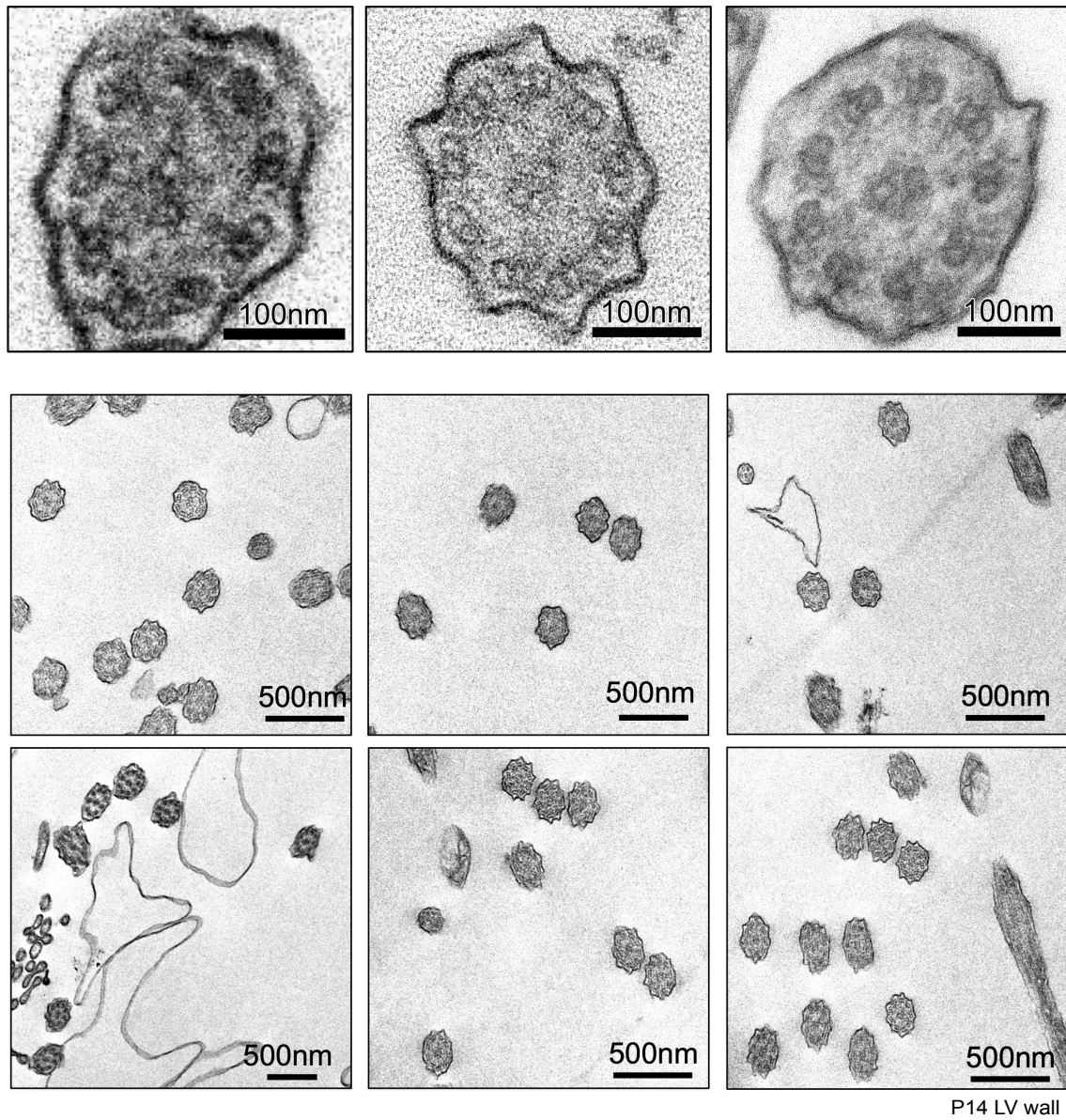


**Fig. S5. TEM images in P14 *Kif6<sup>p.G55fs</sup>* mice, related to Figure.4**

TEM images were taken from three different *Kif6<sup>p.G55fs</sup>* mice LV walls at P14.

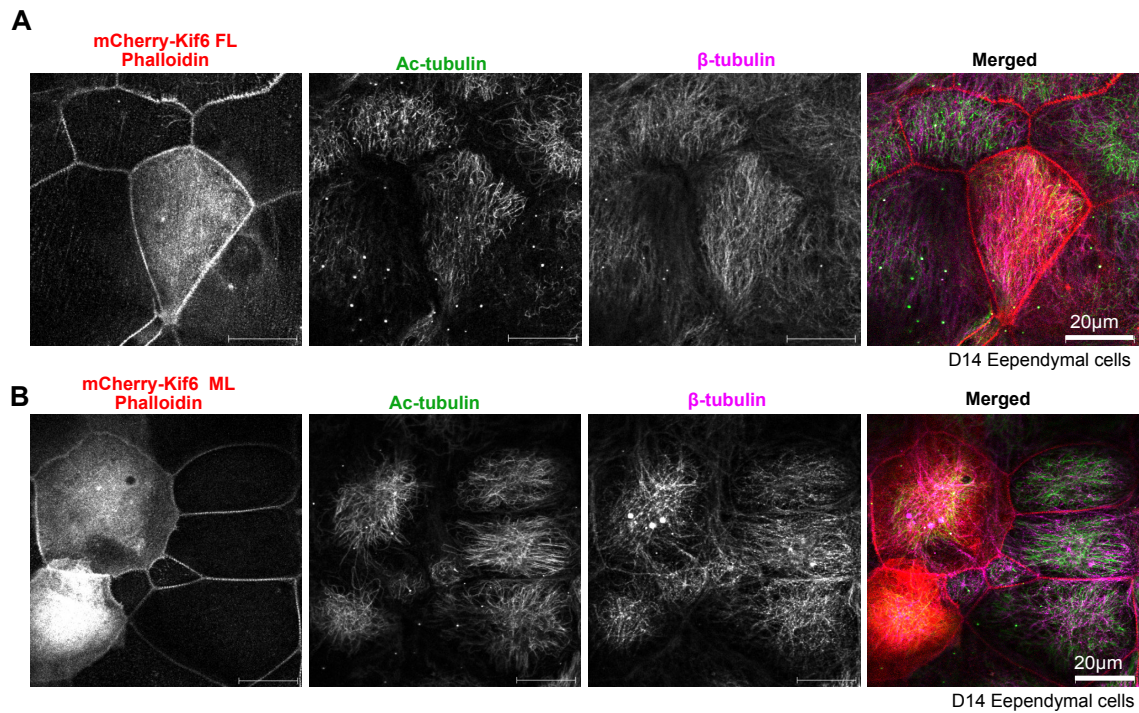
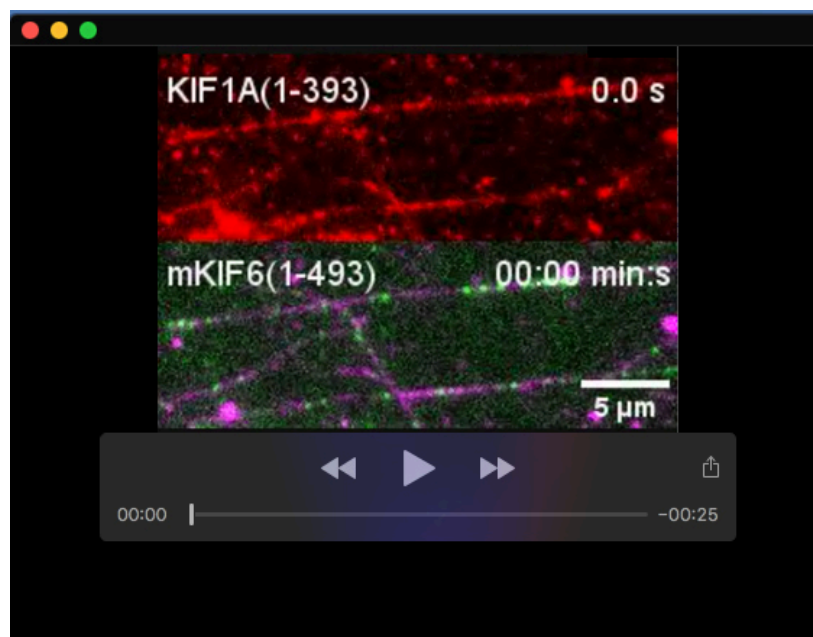


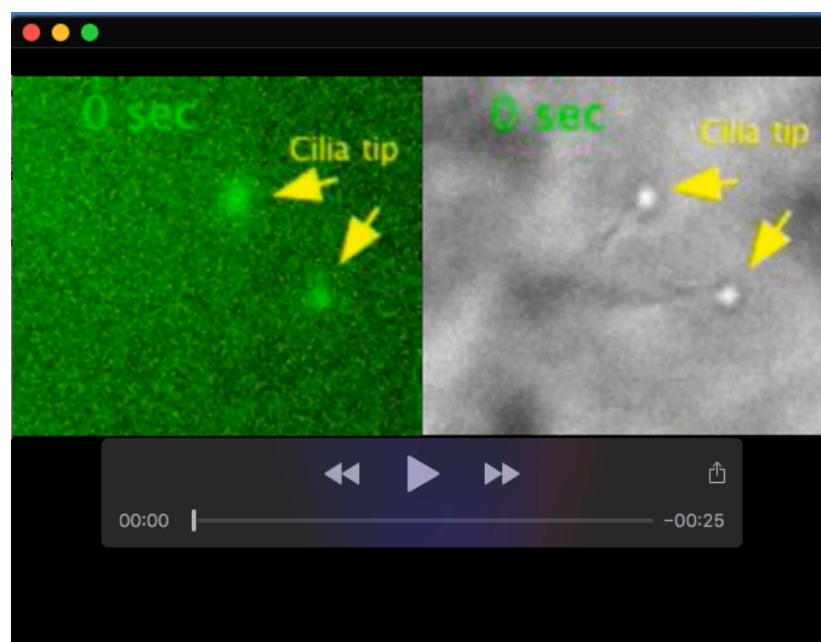
**Fig. S6. Kif6 did not affect overall appearance of microtubules, related to Fig. 5.**

(A, B) Representative images of immunostaining with Ac-tubulin (green) and  $\beta$ -tubulin (magenta) in mCherry-Kif6 FL (A) or mCherry-Kif6 ML (B) expressing D14 ependymal cell.



**Movie 1. Movement of mKIF6(1-493)-mNG and KIF1A (1-393)-LZ-HaloJFX554 7 along taxol-stabilized microtubules *in vitro*, shown in Fig. S3B.**

Cell lysates from COS-7 cells expressing mKif6(1-493)-mNG (green) or KIF1A (1-393)-LZ-HaloJFX554 (red) were added to a flow cell containing HiLy647-labeled taxol-stabilized microtubules (magenta). Images of KIF1A (1-393) were acquired at 1 frame every 100 ms for 61 frames and then images of KIF6(1-493) on the same microtubules were acquired at 1 frame every 3 s for 61 frames. The display rate of the movie is 30 fps.



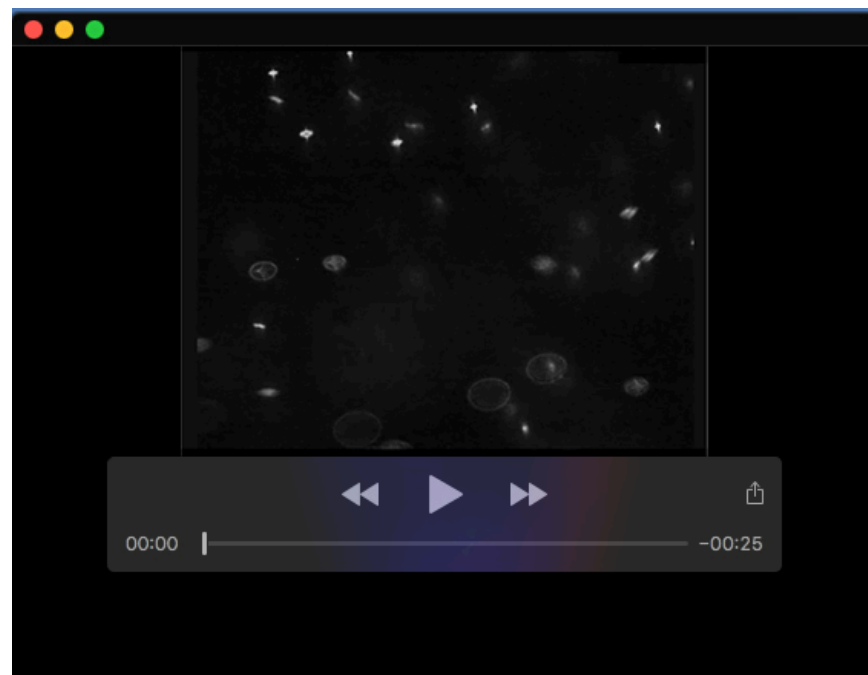
**Movie 2. Live imaging of mKif6 (1-493)-mNG at a developing ependymal cilium, shown in Fig. 1G.**

mKif6 (1-493)-mNG was transfected in D5 ependymal cell, and mKif6 (1-493)-mNG at short developing cilia was imaged at D7. Time-lapse imaging was acquired at 1 frame every 5s for 60 frames. The display rate of the movie is 3 fps.



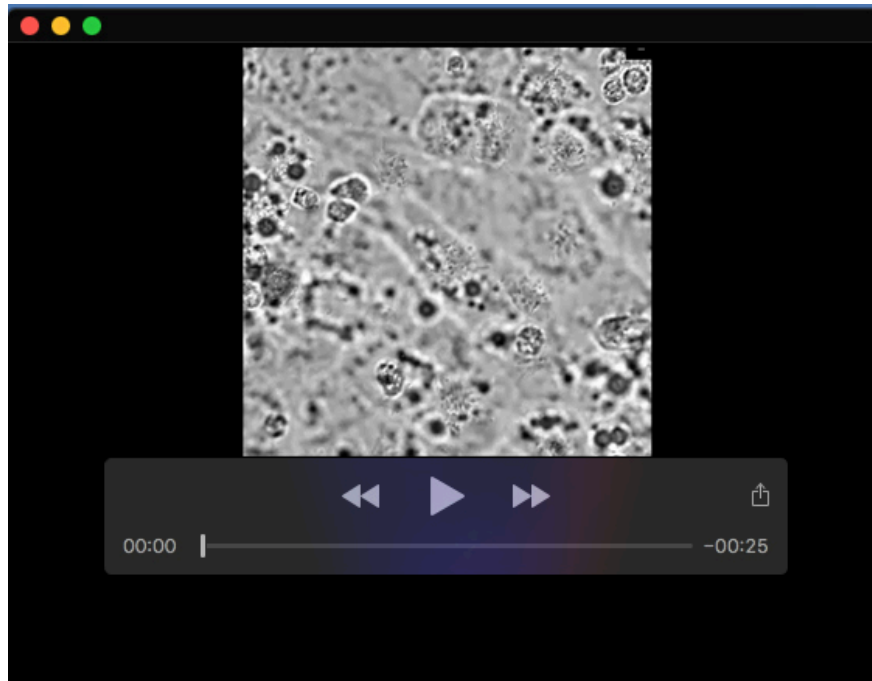
**Movie 3. Beads migration on WT LVW, shown in Fig. 3E.**

Fluorescent microsphere was placed on D12 WT LV wall. The beads migration was recorded in 10 fps for 10sec.



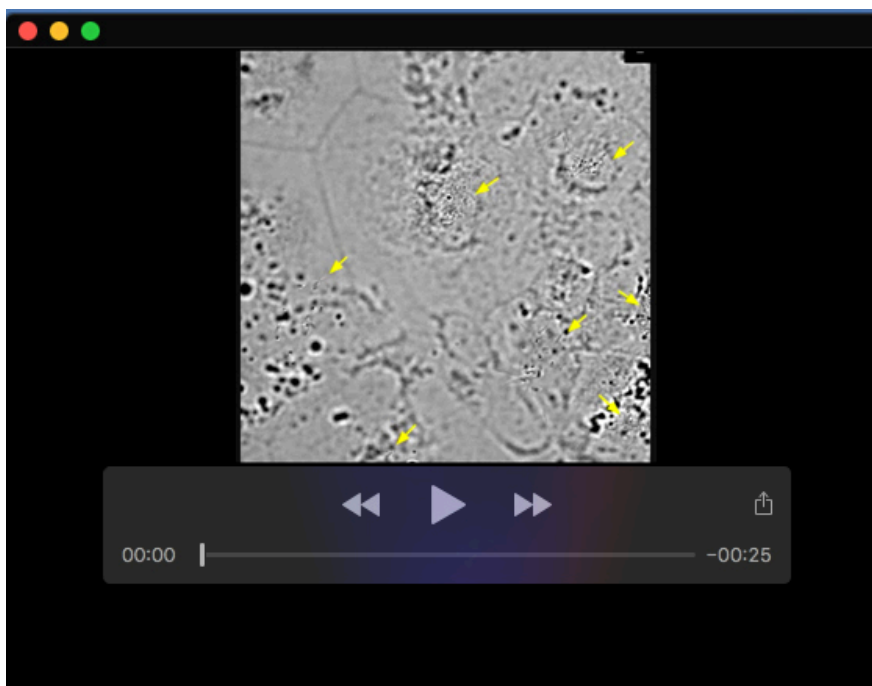
**Movie 4. Beads migration on *Kif6*<sup>p.G555fs</sup> LVW, shown in Fig. 3E.**

Fluorescent microsphere was placed on D12 *Kif6*<sup>p.G555fs</sup> LV wall. The beads migration was recorded in 10 fps for 10sec.



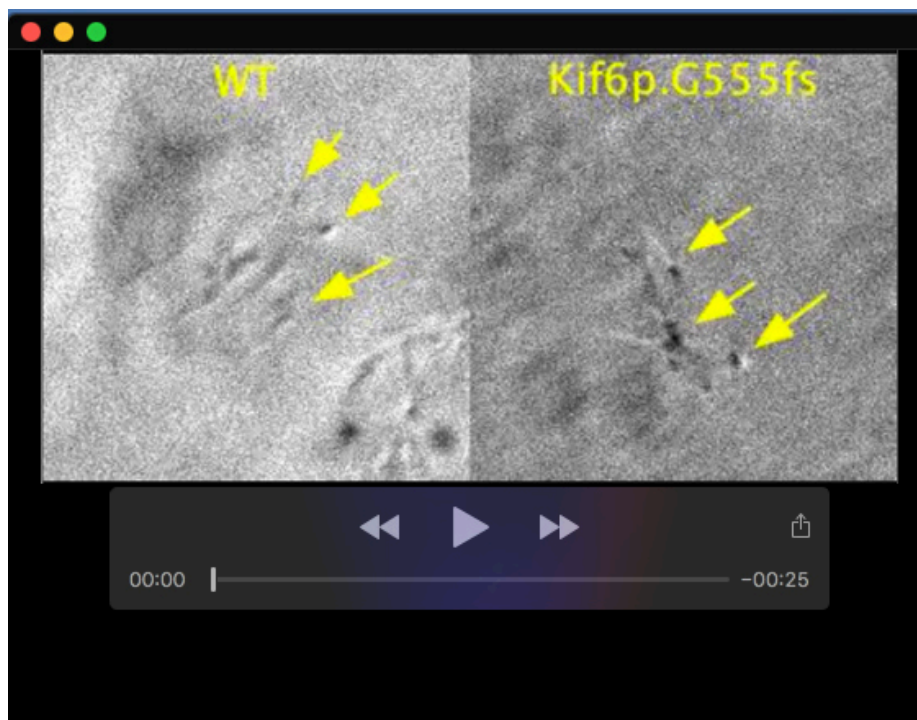
**Movie 5. Live imaging of WT endymal cell cilia at D14.**

Primary cultured endymal cells form WT LV walls were cultured on glass-bottom dish. Time-lapse imaging of DIC was acquired at 47 fps for 2 sec.



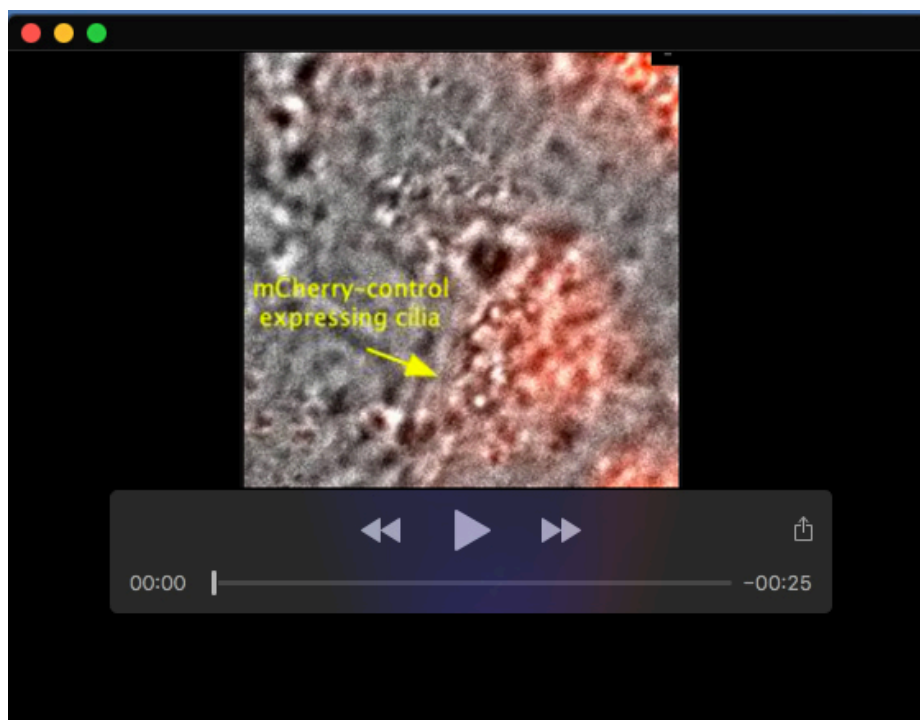
**Movie 6. Live imaging of *Kif6*<sup>p.G555fs</sup> endymal cell cilia at D14.**

Primary cultured endymal cells form *Kif6*<sup>p.G555fs</sup> LV walls were cultured on glass-bottom dish. Time-lapse imaging of DIC was acquired at 47 fps for 2 sec. Arrows indicate cilia on endymal cells.



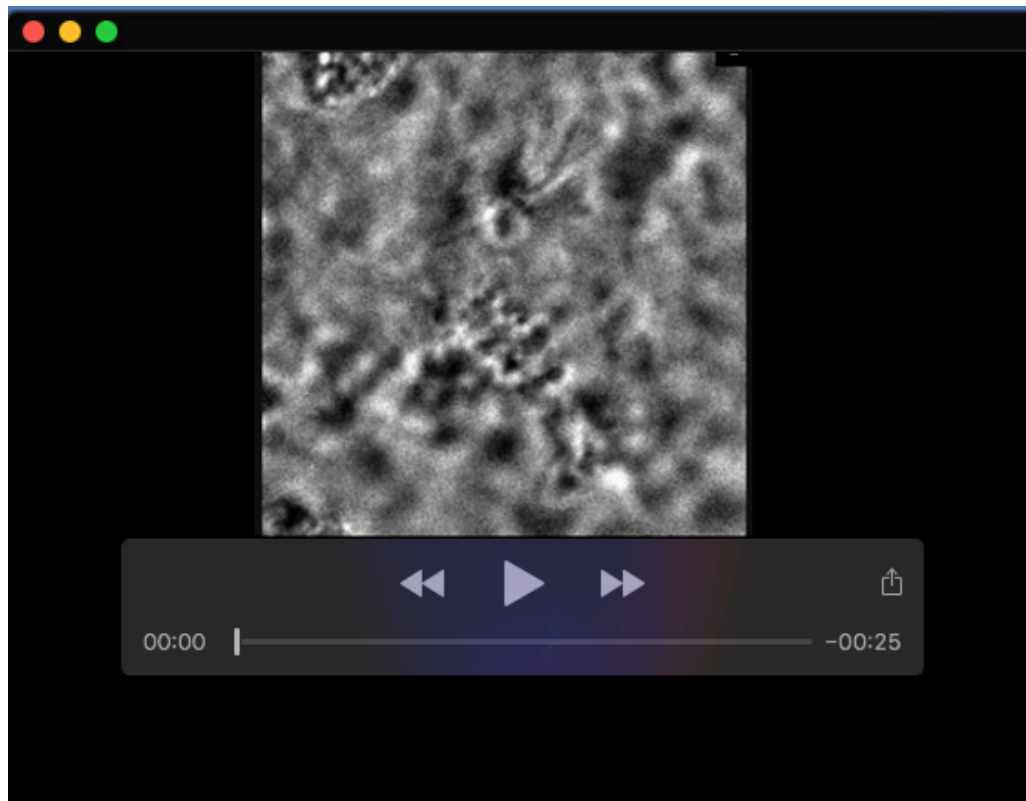
**Movie 7. Live imaging of WT (left) and *Kif6*<sup>p.G555fs</sup>**

Primary cultured endodermal cells from WT or *Kif6*<sup>p.G555fs</sup> LV walls were cultured on glass-bottom dishes. Time-lapse imaging of DIC was acquired at 95 fps for 0.5 sec. Arrows indicate cilia on each endodermal cell.



**Movie 8. Live imaging of mCherry-expressing endodermal cell cilia at D14, related to Fig. 3J.**

Primary cultured endodermal cells from WT LV walls were cultured on glass-bottom dishes and transfected with mCherry at D12. At D14, time-lapse imaging of DIC was acquired at 190 fps for 2 sec. mCherry signal with DIC image is shown in the first frame.



**Movie 9. Live imaging of mCherry-Kif6-ML-expressing ependymal cell cilia at D14, related to Fig. 3J.**

Primary cultured ependymal cells from WT LV walls were cultured on glass-bottom dishes and transfected with mCherry-Kif6-ML at D12. At D14, time-lapse imaging of DIC was acquired at 190 fps for 2 sec. mCherry signal with DIC image is shown in the first frame.